NASA Technical Paper 3278

ATCOM Technical Report 93-A-003

1993

Flight Investigation of the Effect of Tail Boom Strakes on Helicopter Directional Control

Henry L. Kelley and Cynthia A. Crowell
Joint Research Program Office
Aeroflightdynamics Directorate
U.S. Army Aviation and Troop Command
NASA Langley Research Center
Hampton, Virginia

Kenneth R. Yenni
Langley Research Center
Hampton, Virginia

Michael B. Lance
Lockheed Engineering & Sciences Company
Hampton, Virginia

NASA
National Aeronautics and Space Administration
Office of Management
Scientific and Technical Information Program

Summary

A joint U.S. Army/NASA flight investigation was conducted utilizing a single-rotor helicopter to determine the effectiveness of horizontally mounted tail boom strakes on directional controllability and tail rotor power during low-speed, crosswind operating conditions. Three configurations were investigated: (1) baseline (strakes off), (2) single strake (strake at upper shoulder on port side of boom), and (3) double strake (upper strake plus a lower strake on same side of boom). The strakes were employed as a means to separate airflow over the tail boom and change fuselage yawing moments in a direction to improve the yaw control margin and reduce tail rotor power. Crosswind data were obtained in 5-knot increments of airspeed from 0 to 35 knots and in 30° increments of wind azimuth from 0° to 330°. At the most critical wind azimuth and airspeed in terms of tail rotor power, the strakes improved the pedal margin by 6 percent of total travel and reduced tail rotor power required by 17 percent. The increase in yaw control and reduction in tail rotor power offered by the strakes can expand the helicopter operating envelope in terms of gross weight and altitude capability. The strakes did not affect the flying qualities of the vehicle in forward flight at airspeeds between 35 and 100 knots.

Introduction

Single-rotor helicopters sometimes experience minimal yaw control margins and, in some cases, complete loss of yaw control during low-speed crosswind operating conditions (refs. 1–7). Meeting satisfactory yaw control criteria remains a difficult problem for the designer, in part because of numerous contributing factors that make up the total requirement for yaw control. These factors include fuselage aerodynamic yawing moments, main rotor torque, yaw maneuver requirements, and external disturbances such as ambient winds and self-generated effects (downwash, ground recirculation effects, and stability and control cross coupling). In addition, helicopters experience an increase in installed engine power and gross weight over their life cycle, which reduces yaw control margin because of an attendant increase in main rotor torque. A number of investigations have been conducted to define tail rotor performance and directional handling-quality characteristics. The results from some of these investigations are available in references 8–16.

Results from a wind-tunnel investigation (ref. 17) quantified the importance of the fuselage contribution to low-speed yaw control requirements. Analyses of the data indicated that the aerodynamic side forces on the tail boom are a significant portion of the yaw control requirement. For example, estimates based on the model data indicated that the fuselage yawing moment could require on the order of 10 percent of the total yaw control authority. It was reasoned that the tail boom aerodynamic side force was a major contributor to the fuselage yawing moment. As a means of reducing the undesirable fuselage yawing moment, the idea of a spoiler or strake placed along the boom was proposed (ref. 18). Subsequent wind-tunnel investigations (refs. 19 and 20), performed on large-scale two-dimensional cross-sectional shapes of representative U.S. Army helicopter tail booms, clearly indicated that adverse aerodynamic side forces could be generated by the boom and that strakes were useful in reducing these forces. Several flight efforts in the United States and abroad have been conducted to evaluate the effect of tail boom strakes (refs. 21–24). In addition, means to reduce the adverse effects of boom aerodynamic forces on main rotor and tail rotor power are offered through cross section shape design (ref. 22).

A flight investigation utilizing an instrumented single-rotor helicopter (fig. 1) was conducted jointly by the U.S. Army Aeroflightdynamics Directorate and the NASA Langley Research Center in an effort to obtain flight data to augment wind-tunnel results. Data were obtained on three configurations: (1) baseline (research helicopter without strakes), (2) single strake (strake located longitudinally at the upper shoulder of the port side of the boom), and (3) double strake (upper strake plus a lower longitudinally mounted strake on same side of the boom). Low-speed crosswind data were obtained in 5-knot increments of airspeed V from 0 to 35 knots and in 30° increments of wind azimuth ψ from 0° to 330°. Increments in wind azimuth of 15° were investigated where abrupt or significant changes in flying qualities and performance were observed. A limited amount of testing that yielded qualitative results was conducted in forward flight, including climbs, descents, left and right turns, and autorotation. A summary of the results of the flight investigation, the major part of which was directed toward tail rotor power required, yaw control margin, and general handling-quality characteristics as influenced by the tail boom strakes, is presented. Qualitative assessment is given in the form of pilot commentary.

Symbols

b	maximum width of tail boom cross section (wind-tunnel model), ft
BS	tail boom station, in.

C_y	section side-force coefficient, $\frac{\text{Side force per unit length}}{bq}$ (positive right)
C_z	section normal-force coefficient, $\frac{\text{Longitudinal force per unit length}}{bq}$ (positive down)
P	mean tail rotor power, hp
P_σ	standard deviation for tail rotor power, hp
q	dynamic pressure, $\frac{1}{2}\rho v^2$, lb/ft^2
Q_{TR}	tail rotor torque, in-lb
r	aircraft angular yawing velocity, deg/sec
t	time, sec
v	free-stream velocity in tunnel, ft/sec
V	airspeed, knots
ΔP	change in mean tail rotor power compared with baseline, hp
ΔP_{ave}	change in mean tail rotor power compared with baseline averaged over the azimuth range (0°−330°), hp
δ	mean pedal control position (filtered), in.
δ_σ	standard deviation for pedal position, in.
ρ	free-stream air density, slugs/ft^3
ϕ	angle of flow incidence in plane normal to axis of two-dimensional wind-tunnel model, deg
ψ	wind azimuth relative to nose of helicopter, increasing clockwise as viewed from above (0° is a headwind, 90° is a right crosswind, etc.), deg

Crosswind Design and Handling-Quality Considerations

During low-speed, crosswind flight, aerodynamic forces on the tail boom are affected by several factors such as main rotor and tail rotor wakes, ambient winds, maneuvers, ground effects, and the helicopter geometry. Over the years, single-rotor helicopters encounter low-speed directional control problems that degrade handling qualities and mission performance (refs. 2, 3, 5, 6, and 7). Although sideward flight operational requirements vary, many military designs call for a capability to hover in winds from any azimuth at speeds from 0 to 35 knots with a 10-percent pedal control margin remaining at the most critical azimuth and speed. Recent military requirements call for the ability to perform rapid aircraft heading changes in winds of 45 knots from the most critical direction, while civilian requirements call for a 17-knot capability with winds from the critical azimuth. During design, the tail rotor is sized to balance main rotor torque and directional stability moments of the fuselage/tail rotor combination, to provide a sufficient margin for flight maneuvers, and to compensate for ambient wind effects. Demands on tail rotor thrust increase with increasing gross weight and density altitude because of the greater antitorque requirement of the higher gross weight vehicle and the decreasing efficiency of the tail rotor in lower density air. Some of the installation design factors that affect tail rotor thrust are tail rotor/vertical fin blockage, distance between the fin and the plane of the tail rotor, and vertical and horizontal placement of the tail rotor relative to the main rotor. Of course, the design of the tail rotor itself is important in terms of thrust capability. These considerations, however, fall outside the scope of this investigation.

Generally, in right sideward flight as airspeed is increased, the requirement for tail rotor thrust is increased. Conversely, in left sideward flight as airspeed is increased, the requirement for tail rotor thrust decreases to zero and then, at some point, the tail rotor must thrust in the opposite direction. The static-directional stability of the fuselage/tail rotor combined is the major factor that influences this characteristic.

In trimmed right sideward flight, the tail rotor operates in what is termed the normal working state, where the inflow to the tail rotor is in the same direction as the induced velocity produced by the tail rotor, which results in smooth, steady operation and no handling problems. The problem normally associated with right sideward flight is insufficient yaw control caused by either insufficient tail rotor pitch travel or tail rotor aerodynamic stall. The wind azimuth where this problem occurs has been found to be vehicle configuration dependent and generally occurs at $60° \leq \psi \leq 105°$. For the helicopter used in this investigation, it occurred at $\psi = 60°$. The term *configuration dependent* relates to factors specific to a particular helicopter design such as tail rotor vertical placement; height of the main rotor relative to the tail boom and tail rotor; shape, size, and location

of the tail boom; and location and direction of the engine exhaust relative to the tail boom. Another problem that can occur in right ($30° \leq \psi \leq 80°$) and left ($280° \leq \psi \leq 330°$) sideward flight is ingestion of the main rotor wake rollup into the tail rotor. This can cause large and rapid changes in aircraft heading. Whether this phenomenon occurs on a particular helicopter design, or at precisely what wind azimuth it occurs, is also configuration dependent.

In left sideward flight, the handling qualities in a portion of the sideward flight speed and azimuth envelope are characterized by aircraft unsteadiness and the inability of the pilot to hold aircraft trim, particularly aircraft heading. This unsteadiness normally occurs at $240° \leq \psi \leq 300°$ and is caused by the tail rotor operating in the vortex-ring state, where the wind velocity approaching the tail rotor is about one to two times the induced velocity of the tail rotor. The vortex-ring state is characterized by the absence of a well-defined slipstream through the rotor and by large recirculating flows through the rotor. The result is rapidly fluctuating yawing moments that make precision heading control for the pilot virtually impossible.

Finally, yawing moments from the static-directional stability contribution of the fuselage/tail rotor combination create what is commonly termed weathercock stability and produce the moments that tend to turn the nose of the helicopter into the wind. For example, in a tail wind, the helicopter experiences a static-directional instability that requires constant pedal control movement by the pilot to maintain aircraft heading. If the pedals are left unattended, the tail of the helicopter will swing 180° in either direction so that the nose of the aircraft points into the wind. There are also factors caused by ground effects that affect crosswind handling characteristics, but these will not be discussed herein.

Wind-tunnel investigations (refs. 19 and 20) performed on typical helicopter tail boom cross-sectional shapes clearly indicated that rotor downwash could combine with crosswinds (modeled by airflow in the tunnel) to produce right yawing moments in right sideward flight. When this occurs, additional tail rotor thrust is required to trim the aircraft. During stringent flight conditions, such as high gross weight or high density altitude when little or no yaw control margin remains, loss of yaw control may occur. It was also determined during the wind-tunnel investigations that a strake placed longitudinally along the upper shoulder of the model boom was effective in disrupting the airflow over the boom. This disruption of the flow significantly changes the magnitude of the side force. In figure 2, an increase in side-force coefficient C_y (from negative to positive values) indicates a change in boom side force in a favorable direction (reduced tail rotor thrust). Also, a positive increase in the normal-force coefficient C_z indicates an unfavorable increase in boom download. Based on the results in figure 2, the overall effectiveness of the single- and double-strake (a second strake placed longitudinally along the boom, ref. 20) configurations would be expected to be comparable in right sideward flight (comparable values of C_y at positive values of ϕ). The results from a double-strake configuration indicated promise in extending the improvement in side force well into left sideward flight ($-45° < \phi < -10°$) as well as reducing download over a portion of the range of angles investigated ($-35° < \phi < -20°$) (fig. 2).

The size and angular placement of the upper and lower strakes used in the present investigation were derived from experience during the same wind-tunnel investigation, although a detailed parametric study of the effects of strake height and angular location was not made. The strake height of 3 in. used in this investigation is conservative and was selected to ensure that the flow did not reattach to the boom; however, the strake height required is a function of boom depth (including the shaft cover). More detailed experiments (unpublished) performed by industry have determined that the strake height should be 6 7 percent of the boom depth, including the shaft cover. For this investigation, the height was 7 percent and 12 percent at the most forward and most rearward points on the boom, respectively. Of course, it is important to minimize the height in order to minimize download, and a set of strakes tapered in height was designed and fabricated, but only qualitatively evaluated. It is important that the download penalty on the main rotor (typical power loading of about 8 lb thrust/hp) be more than offset by the side-load benefit gained through the strake unloading the tail rotor (typically about 4 lb thrust/hp). The strake should include as much of the length of the boom as practical and extend rearward beyond the normal main rotor wake location to account for movement of the wake due to forward speed. Both wind-tunnel and flight experiments on specific helicopter designs are desirable when considering the use of strakes.

Apparatus and Procedure

Test Helicopter

The test helicopter used in this investigation was a civil version of a turbine-powered vehicle that is representative of a medium weight, utility-class helicopter. This helicopter series has been in service

for about 35 years, and the model used herein was a Bell model 204B. It has a two-bladed, 48-ft-diameter, teetering-main-rotor system with a gyro stabilizer bar. Figure 1(a) shows a photograph of the test helicopter, and table I lists its physical characteristics. A three-view sketch of the basic helicopter showing some of the principal dimensions is given in figure 1(b). Takeoff weight for this investigation varied from about 8000 to 8300 lb, depending on the correction in weight needed to match a reference baseline density ratio based on aircraft gross weight and density altitude. The helicopter was powered by a single free-turbine engine with 1100 shaft hp. No electronic stability augmentation system was used on the helicopter. The pilot's cockpit controls included the conventional cyclic stick, rudder pedals, and collective stick, which were powered by an irreversible hydraulic boost system. Adjustable friction devices were used with the cyclic stick and the collective stick to provide control system feel forces to the pilot. The pedal controls had no friction device. Control force centering was available in the cyclic and directional controls but was not used because most of the test flying required constant out-of-trim conditions. The horizontal stabilizer was connected to the longitudinal cyclic control and was rigged to result in a positive longitudinal cyclic control position gradient.

Strakes

The installation of the upper and lower strakes on the test helicopter tail boom is illustrated in figure 3. The strakes were mounted on the port side of the boom. The three configurations investigated include: (1) baseline (no strakes attached); (2) single strake (upper strake installed); and (3) double strake (upper and lower strakes installed). The 3-in-high strakes were fabricated from 0.06-in-thick 6061-T6 aluminum. Both strakes were made in three sections to accommodate longitudinal curvature in the boom. To facilitate attachment and removal during test sequences, machine screws were fastened through holes into self-locking nut plates mounted inside the boom. The height and angular placement of the strakes were based on force and pressure data obtained in the wind-tunnel investigation of reference 20. The precise angular location followed existing rivet lines along the boom to avoid drilling additional holes in the boom.

Instrumentation

Instrumentation onboard the test helicopter measured and recorded aircraft control positions (longitudinal cyclic stick, lateral cyclic stick, pedal, and collective stick), tail rotor blade pitch angle, aircraft angular velocities (pitch, roll, and yaw), aircraft normal acceleration, aircraft attitudes (pitch, roll, heading), engine shaft torque, tail rotor output shaft strain, main rotor rotational speed, tail rotor rotational speed, and aircraft airspeed. In forward flight, at airspeeds above 40 knots, aircraft angle of attack and sideslip angle were measured with vanes mounted at the end of the nose boom. The vanes and boom were removed for the hover and low-speed tests. Data were recorded on a pulse code modulation (PCM) system and tape recorders located on instrumentation racks in the passenger seating area behind the pilot and copilot seats (fig. 4). Wool tufts were attached to both sides of the tail boom and videotaped to indicate the airflow conditions with the strakes on and off (fig. 5). The time codes on the PCM data tape and videotape were synchronized. A data coupling device (Acurex 1200B Universal Data Coupler) was used at the tail rotor output drive shaft to telemeter the data signal from strain gauges on the rotating output shaft to the nonrotating side at the 90° tail rotor gearbox (fig. 6). This was the first time such a device had been used on a helicopter flight project at Langley in lieu of a more conventional slip ring assembly. This device was used because the helicopter was utilized for several other projects, making slip ring contact wear a concern.

A pace van (fig. 7) was used to assist the pilot in establishing and maintaining the desired test airspeed during the sideward flight portion of the investigation. The van used a speed-measuring radar device that was accurate to within ±2 mph. A portable weather station was mounted approximately 12 ft above the van bumper on a pole and measured wind velocity, wind direction, air temperature, and barometric pressure. The output from this station was displayed and videotaped along with a time code synchronized with the aircraft PCM data system. A radar altimeter was installed on the aircraft with a cockpit dial readout gauge to assist the pilot in maintaining height above the runway during the sideward flight portion of the tests. Data on/off switches and instrument system status lights were located on a control panel in the cockpit and operated by the copilot during the operation. The PCM data system was set up for 52 080 bits/sec, 10 bits/word, 38 words/frame, and a tape recorder speed of 7½ in/sec that resulted in a data sample rate of 137/sec. The data were not filtered during the data recording or reduction process.

Test Procedure

Generally, data were obtained in 5-knot increments of airspeed between 0 and 35 knots and in 30°

increments of wind azimuth over the entire heading range during the low-speed portion of the investigation. The matrix of speeds and azimuths tested is given graphically in figure 8. In rearward flight at azimuths of 150°, 180°, and 210°, a 30-knot airspeed limit was observed, as required by the operator's manual (ref. 25). Also, in cases where significant parameters were changing rapidly as a function of azimuth, data were taken in 15° increments. During this investigation, azimuth (ψ) is defined as the direction from which the wind is approaching the aircraft. For instance, $\psi = 90°$ would denote a direct right crosswind and $\psi = 0°$ would denote a headwind.

Most of the testing was conducted at the NASA Wallops Flight Facility to take advantage of facilities unique to Wallops, including the airport with three runways and little competing air traffic. The low-speed testing was performed at a landing skid height of 40 ft to achieve a near out-of-ground-effect condition (ratio of rotor height to rotor diameter equal to approximately 1.0). During the initial part of the investigation a laser tracking radar system on the Wallops airfield was utilized to monitor the helicopter height above the runway during acquisition of data to ensure that the pilot was maintaining steady level flight. The pilot utilized a radar altimeter readout (analog dial indication) in the cockpit to assist in maintaining a constant height above the runway and thus minimize power changes due to climbing or descending while taking data. Main rotor power changes associated with climb and descent would affect the pedal position and tail rotor power results. Low wind conditions with the prevailing wind direction aligned with one of the runways were required prior to initiating a data flight. Winds were required to be steady (less than 5 knots) with deviations of ±2 knots and with the direction within ±15° of the operating runway heading. Corrections were then calculated for wind velocity and direction between each pass down the runway, and the pace vehicle speed and aircraft heading were adjusted accordingly to account for the wind. Typically, four to seven data points (constant heading and airspeed) were collected during each pass down the runway while aircraft heading was held constant and airspeed was varied. To take a point, the aircraft was stabilized on a desired test airspeed and a 20-sec record was taken. A typical flight lasted 50–75 min with 40–55 data points collected during each flight. Usually, three flights per day (one flight in each configuration) were performed, with the first flight starting at sunrise to take advantage of low wind conditions. For the total program, 37 test flights were performed, which required 28 flight hours.

In forward flight, the handling-quality characteristics were evaluated with strakes on and off (the three test configurations). Maneuvers performed included slow, level flight accelerations and decelerations (change in airspeed of 1 knot/sec or less) between 35 and 100 knots, left and right 30° banked turns at 60 knots, left and right sideslips to sideslip angles of 30° at 60 knots, 1000 ft/min climb at 60 knots, 1300–1400 ft/min descents at 60 knots, and autorotations at 50, 65, 75, and 85 knots.

Presentation of Results

The data are presented graphically as outlined below:

Figure	Parameters plotted	V, knots	ψ, deg	Comparison
9	Mean pedal position vs. airspeed	0–35	0–330	Baseline vs. single strake vs. double strake
10	Tuft patterns on tail boom	0–35	60	Baseline vs. double strake
12	Yaw rate, pedal position, tail rotor torque vs. time	12±3	300	Baseline vs. double strake
13	Mean tail rotor power vs. airspeed	0–35	0 330	Baseline vs. single strake vs. double strake
14	Mean tail rotor power vs. wind azimuth	5–35	0–330	Baseline vs. single strake vs. double strake
15	Change in mean tail rotor power vs. airspeed	0–35	0–330 (averaged)	Baseline vs. single strake vs. double strake
16	Climbing and descending flight	60	0	Baseline vs. double strake
17	Slow trim-level-flight acceleration and deceleration	35–100	0	Baseline vs. double strake

The data from figures 9 and 13 are tabulated in tables II, III, and IV. Table II contains data from the baseline configuration; table III contains data from the single-strake configuration; and table IV contains data from the double-strake configuration.

Results and Discussion

Effect of Strakes on Mean Pedal Control Position

Mean pedal control position as a function of airspeed is presented in figure 9 for the 3 configurations and 16 wind azimuths investigated. As indicated in table I, the pedal control stops are at ±3.44 in., where +3.44 in. is full left pedal. Also, the tail rotor pitch angle varied linearly with pedal position, and full left pedal resulted in +19.4° of tail rotor pitch and full right pedal resulted in −7.1°. A blade pitch of 0° occurred at 1.6 in. of right pedal. The 10-percent total travel control margin called for in military specifications is shown in the plots.

Right sideward flight. For the baseline configuration, the largest left mean pedal requirements occurred in right sideward flight at $\psi = 45°$, 60°, and 75° and at $V = 10$–25 knots (fig. 9(a)). The peak left mean pedal requirement occurred at $\psi = 60°$ and $V = 20$ knots, where 2.9 in. of left mean pedal were required for trim. This peak value is only about 0.5 in. from the left pedal stop and represents about 93 percent of total pedal travel (as measured from right pedal stop) and violates the 10-percent control margin required for maneuvers by some handling-quality specifications. At these azimuths ($\psi = 45°$, 60°, and 75°) and airspeeds ($V = 10$–25 knots), the normal deviations in pedal motion about the mean value resulted in numerous contacts with the left control stop, and on occasion the pedal was on the stop for up to 1 sec with the aircraft heading drifting slowly from trim.

Operation at conditions that require more engine torque, such as higher density altitude and higher vehicle gross weight, would require full pedal control with no margin for maneuvers. For these conditions, the probability of loss of directional control would be greater. Comparison of the baseline results with the results from the single-strake and double-strake configurations indicated an improvement in the mean pedal control margin by an average of about 0.7 in. at $\psi = 45°$ (single-strake data only), $V = 20$ knots; 0.4 in. at $\psi = 60°$, $V = 20$ knots; and 0.6 in. at $\psi = 75°$, $V = 15$ knots.

At $\psi = 0°$ and $V = 10$–20 knots, an increase in left mean pedal is required (fig. 9) because of the strakes, but it is not critical since the mean pedal control is near midrange (between about ±1 in. mean pedal). The effect of the strakes on mean pedal position is minimal at $\psi = 30°$ and $\psi = 120°$. Although $\psi = 150°$ is not a critical wind azimuth in terms of mean pedal travel near a control stop or pedal activity, there was a significant benefit due to the strakes, particularly at speeds between 25 and 30 knots. In fact, at $V = 27$–28 knots, the average benefit for the single- and double-strake configurations compared with the baseline was about 0.7 in. improvement in mean pedal position. Similar effects of lesser magnitude were noted in the third quadrant at $\psi = 210°$ and 240° for $V = 15$–35 knots. Three-dimensional effects, such as the longitudinal velocity component from the helicopter translational airspeed acting on the boom, may contribute to these results.

Analysis of the tail boom tuft visualization data confirmed that the strakes induced flow separation during the critical right sideward flight condition ($\psi = 45°$, 60°, 75°, 90°; $V = 0$–35 knots). Tuft patterns as observed on the left side of the boom over the speed range of $V = 0$–35 knots and $\psi = 60°$ are illustrated in figure 10 for the baseline and double-strake configurations. Analysis of the tuft data indicated that the results for the single-strake and double-strake configurations were virtually the same for the $\psi = 60°$ azimuth condition. The tufts attached to the boom from approximately the horizontal stabilizer to the rearward end of the boom were not readable primarily because of the small viewing angle of the camera. Note that for the baseline configuration, the tufts indicated attached flow with very little back-and-forth motion of the tufts for all speeds investigated. The effectiveness of the strake configurations in smoothing out the peaks in the curves of the baseline configuration, as illustrated particularly at $\psi = 75°$ and $V = 10$–25 knots (fig. 9), indicates that the peaks are caused by an aerodynamic side force on the tail boom when the boom is "flying" in the main rotor wake.

The strakes caused increasingly larger separated flow areas on the boom at $V = 0$ and 5 knots, and then at $V = 10$–35 knots the entire boom area back to the horizontal stabilizer was separated except for a small corner near the forward end of the strakes. In right sideward flight, at airspeeds above about 25 knots, wake skew angle calculations indicate that the main rotor wake would clear the boom, and the flow on the boom in the baseline configuration would be fully separated because the angle of attack would be about 90°. This did not occur at $\psi = 60°$, as indicated by the tuft pictures

(fig. 10, $V = 25$, 30, and 35 knots). These results are confirmed by the data in figure 9 ($\psi = 60°$), which indicate that the advantage in pedal control position for the double-strake configuration compared with the baseline configuration is retained through 25, 30, and 35 knots.

For a given single-rotor helicopter where directional control is the limiting factor, improvements in pedal control margin afforded by the strakes at the critical right sideward flight azimuth and speed ($\psi = 60°$, $V = 20$ knots for the test helicopter) can expand the operating envelope of the helicopter in terms of gross weight and density altitude. Simple calculations indicate that a 10-percent improvement in pedal control margin (about 0.7 in. for the test helicopter) at the critical condition can improve the operational altitude by about 6000 ft or increase the gross weight capability by about 1700 lb for a UH-1 or an AH-1 class helicopter. A figure taken from an Army helicopter operator's manual (ref. 25) shows areas of reduced directional and longitudinal control margins as a function of translational flight speed and direction, and is presented as figure 11. The data in figure 11 are for the in-ground-effect case and apply to UH-1D/H and EH-1E helicopters. It is also shown in the manual that a 5-percent improvement in pedal control margin will provide an additional 2000 ft of altitude capability or 500 lb of payload.

Left sideward flight. In terms of yaw control margin, the concern in left sideward flight is running out of right pedal during certain flight conditions. In figure 9, right mean pedal position is denoted by negative numbers. High-frequency pedal control activity when the tail rotor is operating in the vortex ring state is also of concern in left sideward flight and will be discussed later. It is helpful to remember that tail rotor pitch is 0° at a pedal position of −1.6 in. and increases linearly to −7.1° at the right pedal stop (3.44 in. right pedal). Therefore as pedal position moves from −1.6 in. to a larger more negative value, the tail rotor power required increases as the tail rotor thrusts in the opposite direction. In rearward flight ($\psi = 180°$ and 210°), little effect from the strakes was noted with the pedals within about 1 in. of the center of travel except at speeds of about 25–30 knots at $\psi = 180°$ and 20–30 knots at $\psi = 210°$, where the strakes caused about a 0.5-in. shift in right pedal compared with the baseline. For the remaining wind azimuths of 240°–330°, the mean pedal positions are closer to the right stop for the strake configurations compared with the baseline except at $\psi = 270°$. The 10-percent control margin (pedal at −2.75 in.) was exceeded for $\psi = 270°$, 285°, 300°, and 315°. The single- and double-strake configurations had generally the same characteristics for $\psi = 270°$, 315°, and 330°, whereas at $\psi = 285°$ and 300° the double-strake configuration requires more right pedal. This effect was probably caused by the increased sideward drag of the boom with strakes installed and should be considered prior to strake application, since it caused an exceedance of the control margin in left sideward flight. Optimization of the strake height (limit height to 6 to 7 percent of boom depth) would likely reduce the requirement for right pedal and help minimize this effect.

Effect of Strakes on Precision Controllability

Disturbances that affect precision controllability of the aircraft include operation of the tail rotor in the vortex ring state, which occurs in left sideward flight at azimuths of about 210° to 330°; ingestion of the main rotor tip vortex into the tail rotor, which occurs when the wind is from the front left or front right quadrants; and weathercock instability of the fuselage, which occurs in rearward flight at azimuths between about 120° and 240°.

With the baseline configuration, the major problem in terms of the pilot's ability to hold the aircraft steady occurred at speeds between 10 and 15 knots at $\psi = 300°$. The addition of either the single strake or the double strake reduced the unsteadiness by about 50 percent according to pilot comment. Time histories (fig. 12) of angular yawing velocity, pedal position, and tail rotor torque with double strakes on and off show reduced amplitude and frequency with the strakes on and thereby confirm the pilot comment. The increased steadiness of the aircraft with strakes on is probably achieved because airflow separation is fixed on the boom so that random separation and reattachment of airflow does not occur.

Effect of Strakes on Tail Rotor Power

The mean tail rotor power required as a function of airspeed is presented in figure 13 for the baseline, single-strake, and double-strake configurations for all azimuths investigated. As expected, the general shapes and trends of the curves are similar to the mean pedal position data shown previously (fig. 9), since tail rotor pitch varies linearly with pedal position.

Right sideward flight. For right sideward flight, the azimuths under discussion are 0° to 150° in figures 13(a) and 13(b). The largest mean tail rotor power requirements in right sideward flight occurred for the baseline configuration at $V = 15$–20 knots and $\psi = 45°$, 60°, and 75° with the peak at $\psi = 60°$ and $V = 20$ knots, where the mean tail rotor power

required was 120 hp with transients (not shown) to 150 hp. A moderately high power level is also noted for the baseline configuration at $\psi = 150°$ and $V = 28$ knots. According to the manufacturer, the maximum continuous power rating for the 90° tail rotor gearbox, located at the tail rotor, is 105 hp. Transients in power above 105 hp are allowed in the operating procedures, and the mechanical condition of the gearbox was monitored through routine maintenance inspection procedures.

At $\psi = 45°$ and $V = 20$ knots (fig. 13), the single strake reduced the mean tail rotor power required from 99 to 78 hp (21 percent). For the critical condition ($\psi = 60°$ and $V = 20$ knots), the strakes reduced the mean tail rotor power required from 120 to 100 hp (17 percent), and for $\psi = 75°$ and $V = 15$ knots (peak condition for baseline at $\psi = 75°$), the strakes reduced the mean tail rotor power required from 108 hp to an average of 83 hp (23 percent). At $\psi = 90°$ and $V = 15$ knots, the strakes reduced the mean tail rotor power required from 89 hp to an average of 76 hp (15 percent).

The trends of the data for $\psi = 0°$, 30°, and 120° (fig. 13) follow the pedal position data and will not be discussed further. At $\psi = 150°$, the significant power benefit over most of the speed range is in agreement with the large pedal benefit afforded by both the single- and double-strake configurations compared with the baseline. In fact, the largest power benefit yielded by the strakes during this investigation occurred at $V = 28$ knots and $\psi = 150°$. For this condition, the single- and double-strake configurations reduced the power required from 91 hp to an average of 60 hp (34 percent). This average reduction of 31 hp was significantly greater than that estimated from the two-dimensional wind-tunnel data of reference 20 (22 hp).

Left sideward flight. For $\psi = 180°$–$330°$ in figures 13(c) and 13(d), the trend of mean tail rotor power as a function of airspeed is generally toward lower power levels as speed increases for the three configurations. As mentioned previously, the most significant problem in left sideward flight was the inability to maintain precision control (particularly at $\psi = 300°$, $V = 10$–15 knots) and the need for an adequate control margin from the right pedal stop. These factors were discussed in the section on the effect of strakes on mean pedal position and will not be reiterated here.

Effects of single-strake versus double-strake configurations. The mean tail rotor power benefit or deficit of the single-strake and double-strake configurations compared with the baseline configuration is given in figure 14 as a function of wind azimuth for airspeeds of 5, 10, 20, 25, 30, and 35 knots. A beneficial mean tail rotor power change that resulted from both the single- and double-strake configurations compared with the baseline is presented as positive values of ΔP in the figure. Recall that the absence of data at $V = 35$ knots between $\psi = 120°$ and 240° was due to an operational limit of 30 knots on the rearward flight airspeed of the test helicopter. The curves for this figure were obtained from the data in figure 13 by noting differences in mean power between the configurations every 5 knots and then fairing through the data points.

Examination of the curves over the entire airspeed and azimuth range (fig. 14) indicates that both the single- and double-strake configurations yield an overall mean tail rotor power benefit. Also, the data indicate that both strake configurations continue to be effective in reducing mean tail rotor power required up to an airspeed of 35 knots. For example, when the baseline boom is no longer immersed in the main rotor wake at airspeeds of 25 knots and above, the angle of attack on the boom would be nearly 90° and fully stalled. Once the baseline boom is stalled, the straked configurations, which are designed to stall the boom, can have little or no further benefit in terms of reducing tail rotor power required compared with the baseline. However, based on these data, the strake configurations remained effective compared with the baseline at least to an airspeed of 30 knots.

Compared with the baseline, the strakes were also beneficial over a larger wind azimuth range than anticipated. The reason for the beneficial peaks in the left and right rear quadrants ($90° \leq \psi \leq 270°$), particularly at $V = 10$–30 knots, is not fully understood at this time. As previously mentioned, three-dimensional effects, such as a longitudinal velocity component from the helicopter translational airspeed, may contribute to these results. For many of the speeds, the peaks in the second wind azimuth quadrant ($90° \leq \psi \leq 180°$) approach the size of the peak in the first quadrant, and at $V = 25$ knots the second peak is slightly larger.

At the critical condition of $\psi = 60°$ and $V = 20$ knots, the single-strake result indicates a larger benefit in mean tail rotor power reduction compared with the double strakes (22 hp versus 18 hp). At the other less critical airspeeds ($V = 5$, 15, 25, and 30 knots), the results shown in the same quadrant indicate that the double strakes yielded a larger mean tail rotor power benefit. In addition to the 20-knot case, the results in the right front quadrant show

that the single strake had the larger mean power benefit at $V = 10$ and 35 knots. Large and rapid changes in the increment in mean tail rotor power at $\psi = 260°$–$330°$ and $V = 10$ and 15 knots are another indication of the unsteadiness and precision control problem discussed previously.

The single- and double-strake configurations were further analyzed by taking the data in figure 14 and averaging the power saved or lost compared with the baseline over the entire azimuth and airspeed range (except 35 knots; recall data were not available for $\psi = 150°$–$210°$). This method approximates integrating the areas under the curves in figure 14. Based on this method of averaging the data, the results (fig. 15) indicate that the double strakes were more effective than the single strake in reducing mean tail rotor power required over most of the airspeed and azimuth range.

Effect of Strakes in Forward Flight

In forward flight, as discussed in the Test Procedure section, standard handling-quality testing techniques were used to evaluate the test helicopter without strakes and with single and double strakes. Maneuvers performed included slow, level flight accelerations and decelerations at airspeeds between 35 and 100 knots, and turns, turn entries, sideslips, and climbs and descents at 60 knots. Also, autorotations with power recovery were performed and included turns during the steady-state descent portion of the autorotation at $V = 50$, 65, 75, and 85 knots. According to pilot comment, the strakes had no discernible effects on aircraft handling qualities in forward flight at speeds between 35 and 100 knots. This result agrees with qualitative flight experience with a Westland Sea King helicopter that employed a single upper strake (ref. 22).

Quantitative results from two of the runs are presented in figures 16 and 17 for the baseline and double-strake configurations. Figure 16 includes climbing flight for the first half of the run and descending flight for the second half of the run. In figure 16, the major differences between the baseline and double-strake configurations in terms of pedal position, tail rotor blade angle, and tail rotor power resulted from a rate of climb of 1300 ft/min for the double-strake configuration compared with 1000 ft/min for the baseline configuration (rate of climb information based on pilot comment). This was also reflected in the engine shaft power data where nearly 120 more horsepower were used to initiate the climb in the first 15 sec of the time history. The remaining parameters are in agreement with pilot comment, which indicated no discernible differences in forward flight due to the strakes. The results in figure 17 agree with pilot comment except for differences in pedal position, longitudinal stick position, tail rotor blade angle, collective stick position, and engine shaft power caused by the pilot initiating the maneuver with a larger initial pitch control input (see pitch attitude, fig. 17) for the double-strake case. The remaining parameters are in close agreement for the baseline/double-strake comparison.

Concluding Remarks

A joint NASA/Army flight investigation was conducted to evaluate the effects of horizontally mounted tail boom strakes on the directional controllability and tail rotor power of an instrumented, medium size, single-rotor helicopter during low-speed, crosswind operating conditions. Data were obtained on three configurations: (1) baseline (strakes off), (2) single strake (strake located longitudinally at the upper shoulder on the port side of the boom), and (3) double strake (upper strake plus a lower longitudinally mounted strake also on the port side of the boom). Based on the analyses of the data obtained during this investigation in conjunction with pilot comments, the following concluding remarks are given:

1. For the baseline configuration, a maximum mean tail rotor power of 120 hp was measured at $\psi = 60°$ and $V = 20$ knots; the mean pedal position was within 7 percent of the left control stop, and during excursions about the mean, the pedal was occasionally on the stop. With the addition of the single and double strakes, the mean pedal margin was increased by about 0.4 in. (6 percent of total travel) and the mean tail rotor power required was reduced from 120 to 100 hp (17 percent). Improvements were also measured at other azimuths up to a maximum mean tail rotor power reduction of 34 percent averaged for the double-strake and single-strake configurations.

2. When power differences due to the strakes were averaged over the azimuth range, the double strake was more effective than the single strake over most of the low-speed envelope. Analysis of tail boom tuft videos confirmed that the strakes induced flow separation.

3. In left sideward flight ($\psi = 300°$, $V = 10$–15 knots), a marked increase in aircraft unsteadiness and difficulty of precision control of aircraft heading were noted. According to pilot comment, the addition of strakes improved these effects by 50 percent. However, in left sideward flight, the

addition of the strakes caused the right pedal control margin to exceed the 10-percent control limit but the right pedal stop was not contacted.

4. The strakes had no discernible effects on aircraft handling qualities in forward flight at speeds between 35 and 100 knots.

NASA Langley Research Center
Hampton, VA 23681-0001
January 8, 1993

References

1. Connor, W. J.: The Huey Cobra in Vietnam. *1968 Report to the Aerospace Profession, Tech. Review,* vol. 9, no. 2, Soc. of Experimental Test Pilots, 1968, pp. 25 32.

2. Nagata, John I.; and Buss, Marvin W.: *Army Preliminary Evaluation of the AH-1G Tractor Tail Rotor Modification.* USAASTA-68-37, U.S. Army, June 1969. (Available from DTIC as AD 860 943.)

3. Amer, K. B.; Prouty, R. W.; Walton, R. P.; and Engle, J. E.: Handling Qualities of Army/Hughes YAH-64 Advanced Attack Helicopters. Preprint No. 78-31, *34th Annual National Forum,* American Helicopter Soc., May 1978.

4. Tail Rotor Breakaway. *Helicopter Safety Bulletin,* Flight a Safety Foundation, Inc. (Arlington, Virginia), July/ Aug. 1980.

5. Gerdes, Walter H.; Jackson, Michael E.; and Beno, Edward A.: *Directional Control Developmental Experiences Associated With the UH-60A Utility Helicopter.* U.S. Army, May 1983. (Available from DTIC as AD B075 534L.)

6. MacMullin, Robert; Downs, Gary T.; Tavares, Edward; Lawrence, John S.; Todd, Loren L.; and Carmona, Waldo F.: *Preliminary Airworthiness Evaluation of the AH-1S (Modernized Cobra) With the Hellfire, TOW, and Stinger Missiles Installed.* USAAEFA Proj. No. 84 11, U.S. Army, Oct. 1984. (Available from DTIC as AD A160 862.)

7. Cassil, Charles E.; and Lockwood, Roy A.: *Preliminary Airworthiness Evaluation of the UH-1H Helicopter With the T53-L-703 Engine Installed.* USAAEFA Proj. No. 84-25, U.S. Army, June 1986. (Available from DTIC as AD A182 369.)

8. Lynn, R. R.; Robinson, F. D.; Batra, N. N.; and Duhon, J. M.: Tail Rotor Design. Part I: Aerodynamics. *J. American Helicopter Soc.,* vol. 15 no. 4, Oct. 1970, pp. 2 15.

9. Huston, Robert J.; and Morris, Charles E. K., Jr.: *A Wind-Tunnel Investigation of Helicopter Directional Control in Rearward Flight in Ground Effect.* NASA TN D-6118, 1971.

10. Kolesar, Charles E.: *1/4.85 Scale Full Powered Model: Wind Tunnel Test Results.* D179-10413-1 (Contract DAAJ01-1-73-C-0007(P40)), Boeing Vertol Co., Apr. 26, 1974.

11. Wiesner, Wayne; and Kohler, Gary: Tail Rotor Performance in Presence of Main Rotor, Ground, and Winds. *J. American Helicopter Soc.,* vol. 19, no. 3, July 1974, pp. 2 9.

12. Yeager, William T., Jr.; Young, Warren H., Jr.; and Mantay, Wayne R.: *A Wind-Tunnel Investigation of Parameters Affecting Helicopter Directional Control at Low Speeds in Ground Effect.* NASA TN D-7694, 1974.

13. Sheridan, Philip F.; and Wiesner, Wayne: Aerodynamics of Helicopter Flight Near the Ground. *33rd Annual National Forum,* American Helicopter Soc., 1977, pp. 77.33-04-1 77.33-04-11. (Available as Preprint No. 77.33-04.)

14. Sheridan, Philip F.: *Interactional Aerodynamics of the Single Rotor Helicopter Configuration. Volume I Final Report.* USARTL-TR-78-23A, U.S. Army, Sept. 1978. (Available from DTIC as AD A060 389.)

15. Sheridan, Philip F.; and Smith, Robert P.: Interactional Aerodynamics A New Challenge of Helicopter Technology. *35th Annual National Forum,* American Helicopter Soc., Inc., 1979, pp. 79-59-1 79-59-15. (Available as Preprint No. 79-59.)

16. Blake, Bruce B.; Hodder, David St. J.; and Hanker, Edward J.: *Wind Tunnel Investigation Into the Directional Control Characteristics of an OH-58A Helicopter.* USAAVRADCOM TR-83-D-18, U.S. Army, 1984.

17. Wilson, John C.; and Mineck, Raymond E.: *Wind-Tunnel Investigation of Helicopter-Rotor Wake Effects on Three Helicopter Fuselage Models.* NASA TM X-3185, 1975.

18. Wilson, John C.: Rotorcraft Low-Speed Download Drag Definition and Its Reduction. *Rotorcraft Parasite Drag—Proceedings of the Thirty-First Annual National Forum,* American Helicopter Soc., Inc., 1975, pp. 4-1 4-9.

19. Wilson, John C.; and Kelley, Henry L.: Measured Aerodynamic Forces on Three Typical Helicopter Tail Boom Cross Sections. *J. American Helicopter Soc.,* vol. 28, no. 4, Oct. 1983, pp. 68 71.

20. Wilson, John C.; and Kelley, Henry L.: *Aerodynamic Characteristics of Several Current Helicopter Tail Boom Cross Sections Including the Effect of Spoilers.* NASA TP-2506, AVSCOM TR-85-B-3, 1986.

21. Smith, Robert P.; Leonard, William A.; and Kelley, Henry L.: Limited Flight Investigation of Strakes Mounted on a Helicopter Tail Boom. Paper presented at the U.S. Army Research Office/American Helicopter Society International Conference on Rotorcraft Basic Research (Research Triangle Park, North Carolina), Feb. 19 21, 1985.

22. Brocklehurst, Alan: A Significant Improvement to the Low Speed Yaw Control of the Sea King Using a Tail Boom Strake. *Eleventh European Rotorcraft Forum,* City Univ. (London, England), 1985, pp. 32-1–32-11.

23. Lockwood, Roy A.; Kelly, William A.; and Cason, Randall W.: *Flight Characteristics Test of the UH-60A With Tail Boom Mounted Strake.* USAAEFA Proj. No. 85-07, U.S. Army, Oct. 1986.

24. Wilson, John C.; Kelley, Henry L.; Donahue, Cynthia C.; and Yenni, Kenneth R.: *Developments in Helicopter Tail Boom Strake Applications in the United States.* NASA TM-101496, AVSCOM TM-88-B-014, 1988.

25. *Operator's Manual—Army Models UH-1D/H and EH-1H Helicopters.* TM 55-1520-210-10, Headquarters, Dep. of the Army, May 18, 1979. (This manual supersedes TM 55-1520-210-10, dated Aug. 25, 1971, including all changes.)

Table 1. Physical Characteristics of Test Helicopter

Main rotor:	
Diameter, ft	48
Number of blades	2
Blade chord, in.	21
Airfoil section	NACA 0012
Twist, deg (linear)	−11
Flapping angle range, deg	±10
Blade taper ratio	0
Disc area, ft^2	1810
Solidity	0.0506
Tip speed, ft/sec	815
Normal operating speed, rpm	324
Engine to rotor gear ratio	20.37:1
Tail rotor:	
Diameter, ft	8.5
Number of blades	2
Blade chord, in.	8.4
Airfoil section	NACA 0015
Twist, deg	0
Blade taper ratio	0
Disc area, ft^2	56.7
Solidity	0.105
Blade area, ft^2	5.954
Tip speed, ft/sec	740
Normal operating speed, rpm	1663
Blade pitch angle, deg:	
Full left pedal	+19.4
Full right pedal	−7.1
Delta-three hinge angle, deg	35
Direction of rotation	Bottom blade rearward
General:	
Normal weight (max. gross), lb	8500
Weight (as tested), lb	8200
Empty weight, lb	4600
Overall length, ft	56.1
Overall height, ft	14.6
Landing gear tread, ft	8.4
Power (Lycoming T53):	
Normal, shp	900
Normal, rpm	6600
Takeoff, shp	1100
Maximum-level-flight airspeed, knots	110
Center of gravity (as tested):	
Longitudinal (fuselage station)	131.60
Lateral	−.03
Control travels (from grip centers):	
Lateral stick, in.	±6.17
Longitudinal stick, in.	±6.43
Pedals, in.	±3.44
Collective stick, in.:	
Full up	10.6
Full down	0

Table II. Mean and Standard Deviation Values for Tail Rotor Power and Pedal Position From Data in Figures 9 and 13 for the Baseline Configuration

$\psi = 0°$

V, knots	P, hp	P_σ, hp	δ, in.	δ_σ, in.
0	61.59	4.58	1.13	0.08
5	68.73	7.07	1.31	.17
10	49.77	3.59	.83	.09
15	40.03	3.98	.44	.07
20	30.38	3.60	.00	.10
25	26.65	4.02	−.26	.15
30	24.03	4.04	−.44	.13
35	22.74	3.65	−.52	.10

$\psi = 30°$

V, knots	P, hp	P_σ, hp	δ, in.	δ_σ, in.
0	61.59	4.58	1.13	0.08
5	68.98	4.11	1.35	.08
10	75.22	4.59	1.64	.08
15	78.39	4.12	1.69	.06
20	65.75	4.60	1.35	.10
25	58.07	7.09	1.24	.20
30	59.03	4.44	1.28	.09
35	61.04	3.91	1.34	.10

$\psi = 45°$

V, knots	P, hp	P_σ, hp	δ, in.	δ_σ, in.
0	61.59	4.58	1.13	0.08
5	71.29	4.84	1.41	.11
10	75.88	7.26	1.59	.12
15	90.23	6.86	1.92	.12
20	99.18	11.69	2.51	.21
25	79.35	8.48	2.12	.18
30	72.98	9.81	1.85	.20
35	81.11	8.98	2.13	.19

$\psi = 60°$

V, knots	P, hp	P_σ, hp	δ, in.	δ_σ, in.
0	61.59	4.58	1.13	0.08
8	83.55	5.70	1.79	.14
9	86.61	7.30	1.72	.17
10	86.43	6.92	1.90	.13
15	99.54	12.65	2.22	.22
20	119.64	11.48	2.94	.25
25	98.29	22.22	2.50	.66
30	92.08	19.83	2.38	.52
35	72.87	11.00	1.92	.26

$\psi = 75°$

V, knots	P, hp	P_σ, hp	δ, in.	δ_σ, in.
0	61.59	4.58	1.13	0.08
5	79.06	5.36	1.64	.11
10	94.48	11.37	1.99	.22
15	107.76	11.21	2.36	.18
20	93.80	12.16	2.01	.24
25	76.51	10.25	1.75	.18
30	81.32	6.75	1.89	.10
35	91.33	5.21	2.16	.09

$\psi = 90°$

V, knots	P, hp	P_σ, hp	δ, in.	δ_σ, in.
0	61.59	4.58	1.13	0.08
5	75.34	4.21	1.51	.06
10	80.28	4.31	1.61	.06
15	89.41	10.35	1.82	.17
20	80.44	8.26	1.74	.12
25	75.98	5.63	1.72	.09
30	86.74	5.86	1.99	.11
35	90.46	5.97	2.10	.08

$\psi = 120°$

V, knots	P, hp	P_σ, hp	δ, in.	δ_σ, in.
0	61.59	4.58	1.13	0.08
2	63.72	5.24	1.11	.14
15	71.31	5.02	1.42	.09
20	68.24	6.80	1.41	.14
25	73.53	8.13	1.61	.18
30	78.95	9.52	1.81	.18
35	84.77	9.23	1.98	.18

$\psi = 150°$

V, knots	P, hp	P_σ, hp	δ, in.	δ_σ, in.
0	61.59	4.58	1.13	0.08
8	70.64	6.54	1.27	.18
18	70.27	6.93	1.40	.18
23	75.92	4.93	1.64	.11
28	90.72	5.81	2.02	.13
33	79.77	5.90	1.75	.11

Table II. Concluded

$\psi = 180°$

V, knots	P, hp	P_σ, hp	δ, in.	δ_σ, in.
0	61.59	4.58	1.13	0.08
5	65.72	5.86	1.21	.12
10	49.75	4.48	.73	.13
15	44.80	4.00	.58	.12
20	38.48	4.05	.33	.08
25	35.34	6.93	.20	.23
30	27.33	9.74	−.27	.28

$\psi = 210°$

V, knots	P, hp	P_σ, hp	δ, in.	δ_σ, in.
0	61.59	4.58	1.13	0.08
2	55.10	3.22	.84	.09
8	52.66	4.06	.63	.07
10	55.63	4.81	.65	.12
15	44.03	4.69	.32	.09
20	43.15	6.00	.29	.14
25	29.91	7.26	−.36	.25
30	26.44	7.23	−.60	.31

$\psi = 240°$

V, knots	P, hp	P_σ, hp	δ, in.	δ_σ, in.
0	61.59	4.58	1.13	0.08
2	55.96	4.78	.90	.15
8	50.11	5.53	.65	.20
15	34.12	7.78	−.22	.34
20	25.58	7.09	−.78	.28
25	24.07	8.08	−.82	.46
30	22.56	7.86	−.92	.28
35	11.89	5.46	−1.90	.30

$\psi = 270°$

V, knots	P, hp	P_σ, hp	δ, in.	δ_σ, in.
0	61.59	4.58	1.13	0.08
5	58.18	3.58	1.01	.08
10	29.42	6.58	−.21	.32
15	15.99	4.34	−1.24	.30
20	13.90	3.47	−1.47	.12
25	11.60	4.61	−1.72	.19
30	7.38	3.31	−2.17	.14
35	5.25	3.37	−2.47	.15

$\psi = 285°$

V, knots	P, hp	P_σ, hp	δ, in.	δ_σ, in.
0	61.59	4.58	1.13	0.08
5	55.83	3.98	.94	.09
10	30.74	7.24	−.10	.34
15	15.73	3.94	−1.16	.16
20	13.57	3.66	−1.40	.10
25	11.86	3.76	−1.58	.14
30	6.83	3.43	−2.19	.13
35	3.17	2.53	−2.71	.17

$\psi = 300°$

V, knots	P, hp	P_σ, hp	δ, in.	δ_σ, in.
0	61.59	4.58	1.13	0.08
2	55.80	5.20	.90	.17
8	63.14	8.56	1.30	.33
10	40.91	6.00	.63	.28
15	28.61	6.62	−.23	.34
20	12.32	4.37	−1.59	.21
25	6.44	4.30	−2.39	.27
30	5.38	4.94	−2.71	.17
35	5.92	4.71	−2.65	.20

$\psi = 315°$

V, knots	P, hp	P_σ, hp	δ, in.	δ_σ, in.
0	61.59	4.58	1.13	0.08
5	58.54	5.38	1.03	.12
10	57.60	7.75	1.35	.23
15	31.58	5.21	.07	.21
20	16.04	3.94	−1.07	.23
25	4.49	5.30	−2.06	.17
30	3.38	3.47	−2.14	.22
35	3.79	4.85	−3.09	.21

$\psi = 330°$

V, knots	P, hp	P_σ, hp	δ, in.	δ_σ, in.
0	61.59	4.58	1.13	0.08
2	66.15	5.62	1.19	.11
8	57.57	5.25	.90	.15
10	44.38	7.54	.69	.32
15	36.40	8.64	.22	.40
20	20.85	4.92	−.94	.21
25	14.97	7.76	−1.36	.37
30	6.37	7.14	−2.08	.31
35	5.69	6.83	−2.21	.25

Table III. Mean and Standard Deviation Values for Tail Rotor Power and Pedal Position From Data in Figures 9 and 13 for the Single-Strake Configuration

$\psi = 0°$

V, knots	P, hp	P_σ, hp	δ, in.	δ_σ, in.
0	66.85	6.26	1.36	0.16
4	64.78	7.54	1.32	.18
10	64.04	4.46	1.23	.09
15	45.98	4.07	.64	.12
20	37.75	4.56	.32	.12
25	31.69	3.30	.09	.05
30	27.22	3.54	−.20	.10
35	25.63	3.68	−.33	.13

$\psi = 30°$

V, knots	P, hp	P_σ, hp	δ, in.	δ_σ, in.
0	66.85	6.26	1.36	0.16
4	69.32	7.96	1.43	.22
10	83.98	5.62	1.81	.09
15	87.22	6.33	1.88	.10
20	75.50	6.37	1.74	.14
25	56.64	4.50	1.22	.07
30	55.99	5.44	1.27	.15
35	56.62	5.59	1.23	.13

$\psi = 45°$

V, knots	P, hp	P_σ, hp	δ, in.	δ_σ, in.
13	84.80	6.72	1.58	0.12
15	86.35	9.02	1.72	.24
20	77.61	8.72	1.83	.14
25	68.10	7.53	1.54	.16
30	57.02	8.63	1.04	.22
35	61.73	7.28	1.23	.17

$\psi = 60°$

V, knots	P, hp	P_σ, hp	δ, in.	δ_σ, in.
0	66.85	6.26	1.36	0.16
4	79.74	6.07	1.74	.11
10	97.76	7.38	2.07	.12
15	104.40	11.06	2.27	.19
20	98.03	8.83	2.41	.17
25	81.96	10.64	2.10	.27
30	69.16	7.03	1.68	.16
35	78.17	6.72	1.91	.09

$\psi = 75°$

V, knots	P, hp	P_σ, hp	δ, in.	δ_σ, in.
0	66.85	6.26	1.36	0.16
4	79.57	6.07	1.71	.11
10	98.44	17.83	2.14	.37
15	87.66	8.64	1.97	.19
20	72.45	5.07	1.61	.06
25	75.67	5.11	1.73	.06
30	79.53	5.70	1.90	.08
35	93.58	5.97	2.22	.09

$\psi = 90°$

V, knots	P, hp	P_σ, hp	δ, in.	δ_σ, in.
0	66.85	6.26	1.36	0.16
4	78.42	7.58	1.67	.18
10	75.41	8.82	1.48	.20
15	78.57	5.24	1.58	.09
20	73.93	4.73	1.61	.08
25	80.22	5.84	1.81	.09
30	83.77	7.56	1.94	.12

$\psi = 120°$

V, knots	P, hp	P_σ, hp	δ, in.	δ_σ, in.
0	66.85	6.26	1.36	0.16
4	71.40	7.58	1.45	.18
10	70.27	4.50	1.40	.08
15	69.56	6.00	1.42	.14
20	68.10	5.57	1.44	.09
25	71.75	6.27	1.60	.12
30	86.55	5.92	2.00	.10
35	104.77	7.13	2.43	.09

$\psi = 150°$

V, knots	P, hp	P_σ, hp	δ, in.	δ_σ, in.
0	66.85	6.26	1.36	0.16
4	58.77	5.64	1.07	.13
10	62.55	4.66	1.18	.07
15	60.51	5.11	1.14	.08
20	62.90	5.26	1.22	.07
25	57.65	8.92	1.11	.25
30	65.74	9.25	1.36	.22

Table III. Concluded

$\psi = 180°$

V, knots	P, hp	P_σ, hp	δ, in.	δ_σ, in.
0	66.85	6.26	1.36	0.16
4	55.04	5.46	.99	.14
10	52.43	4.04	.84	.10
15	50.12	5.47	.72	.16
20	40.81	6.41	.39	.16
25	28.59	6.04	−.21	.22
30	26.97	8.45	−.33	.25

$\psi = 210°$

V, knots	P, hp	P_σ, hp	δ, in.	δ_σ, in.
0	66.85	6.26	1.36	0.16
4	53.85	4.25	.97	.10
10	42.91	4.23	.53	.12
12	42.36	5.63	.29	.14
15	38.01	5.51	.07	.19
20	34.21	6.78	−.13	.25
25	22.14	5.83	−.91	.23
30	17.70	5.51	−1.25	.18

$\psi = 240°$

V, knots	P, hp	P_σ, hp	δ, in.	δ_σ, in.
0	66.85	6.26	1.36	0.16
4	54.36	5.58	1.00	.14
12	41.04	5.55	.30	.12
15	20.98	5.11	−1.00	.19
20	18.56	4.79	−1.24	.15
25	15.61	4.30	−1.49	.17
30	10.22	4.59	−1.99	.24
35	8.14	4.53	−2.29	.20

$\psi = 270°$

V, knots	P, hp	P_σ, hp	δ, in.	δ_σ, in.
0	66.85	6.26	1.36	0.16
4	58.44	7.59	1.15	.20
10	25.17	5.66	−.47	.21
15	24.61	5.25	−.49	.26
20	13.89	3.68	−1.44	.12
25	11.35	4.20	−1.71	.16
30	7.18	3.68	−2.18	.17
35	4.72	2.65	−2.48	.18

$\psi = 285°$

V, knots	P, hp	P_σ, hp	δ, in.	δ_σ, in.
0	66.85	6.26	1.36	0.16
4	61.07	7.73	1.25	.21
10	39.82	6.92	.53	.29
15	16.35	3.68	−1.13	.15
20	10.73	3.95	−1.86	.16
25	8.82	4.07	−2.09	.17
30	6.68	3.55	−2.29	.14
35	2.02	1.95	−2.83	.09

$\psi = 300°$

V, knots	P, hp	P_σ, hp	δ, in.	δ_σ, in.
0	66.85	6.26	1.36	0.16
4	58.02	5.03	1.09	.10
10	56.72	6.86	1.20	.22
15	41.57	5.97	.56	.21
20	13.19	6.30	−1.59	.41
25	8.24	6.22	−2.26	.27
30	7.05	5.47	−2.61	.28
35	6.40	7.32	−2.86	.35

$\psi = 315°$

V, knots	P, hp	P_σ, hp	δ, in.	δ_σ, in.
0	66.85	6.26	1.36	0.16
4	65.26	7.56	1.31	.20
10	38.13	5.15	.45	.11
15	25.22	6.34	−.41	.35
20	13.80	4.66	−1.30	.13
25	4.74	4.83	−2.16	.20
30	2.51	2.97	−2.71	.11
35	3.01	3.86	−3.02	.18

$\psi = 330°$

V, knots	P, hp	P_σ, hp	δ, in.	δ_σ, in.
0	66.85	6.26	1.36	0.16
4	63.65	8.19	1.28	.21
10	62.28	11.75	1.49	.34
15	32.42	8.84	.12	.44
20	17.43	8.70	−.87	.46
25	8.60	7.07	−1.85	.24
30	6.53	5.78	−2.15	.16
35	7.56	5.28	−2.20	.17

Table IV. Mean and Standard Deviation Values for Tail Rotor Power and Pedal Position From Data in Figures 9 and 13 for the Double-Strake Configuration

$\psi = 0°$

V, knots	P, hp	P_σ, hp	δ, in.	δ_σ, in.
0	56.24	4.46	0.98	0.10
5	64.28	4.25	1.24	.10
10	65.28	4.01	1.34	.08
15	58.58	3.80	1.18	.06
20	42.25	4.45	.53	.16
25	32.68	3.22	.17	.07
30	26.70	3.11	−.21	.08
35	24.58	3.55	−.32	.14

$\psi = 30°$

V, knots	P, hp	P_σ, hp	δ, in.	δ_σ, in.
0	56.24	4.46	0.98	0.10
5	73.59	4.60	1.51	.11
10	77.69	6.20	1.73	.11
20	71.69	7.30	1.62	.17
25	53.62	4.33	1.15	.08
30	51.38	4.24	1.12	.09
35	51.75	4.52	1.12	.10

$\psi = 60°$

V, knots	P, hp	P_σ, hp	δ, in.	δ_σ, in.
0	56.24	4.46	0.98	0.10
5	70.19	4.99	1.38	.10
10	79.25	5.94	1.81	.08
15	105.70	8.14	2.48	.15
20	102.14	10.00	2.61	.17
25	75.09	12.22	1.89	.37
30	66.54	9.63	1.78	.20
35	76.96	7.06	1.91	.14

$\psi = 75°$

V, knots	P, hp	P_σ, hp	δ, in.	δ_σ, in.
0	56.24	4.46	0.98	0.10
5	83.48	8.22	1.75	.14
10	76.29	5.62	1.58	.12
15	77.64	4.86	1.63	.09
18	78.13	5.12	1.67	.07
23	70.93	3.98	1.60	.06
28	73.23	4.53	1.72	.06
32	83.28	5.84	2.00	.09

$\psi = 90°$

V, knots	P, hp	P_σ, hp	δ, in.	δ_σ, in.
0	56.24	4.46	0.98	0.10
5	79.96	6.33	1.64	.09
10	72.57	5.79	1.45	.13
15	74.07	5.04	1.51	.10
20	72.42	5.21	1.58	.10
25	75.57	4.68	1.73	.07
30	84.49	4.82	2.03	.07
35	88.39	6.27	2.20	.11

$\psi = 120°$

V, knots	P, hp	P_σ, hp	δ, in.	δ_σ, in.
0	56.24	4.46	0.98	0.10
5	70.51	4.39	1.34	.07
10	60.75	4.72	1.14	.08
20	69.79	5.38	1.45	.09
25	71.42	4.98	1.62	.09
30	76.17	6.40	1.80	.12
35	85.81	6.40	2.05	.11

$\psi = 150°$

V, knots	P, hp	P_σ, hp	δ, in.	δ_σ, in.
0	56.24	4.46	0.98	0.10
5	64.45	4.98	1.19	.10
10	53.95	3.88	.88	.10
15	52.42	4.80	.85	.11
20	51.82	6.55	.86	.21
25	54.61	6.41	1.02	.15
30	62.56	5.58	1.23	.08

$\psi = 180°$

V, knots	P, hp	P_σ, hp	δ, in.	δ_σ, in.
0	56.24	4.46	0.98	0.10
5	58.47	4.89	.99	.11
10	51.41	3.46	.89	.06
15	48.95	4.94	.76	.15
20	43.50	7.13	.60	.23
25	39.85	6.14	.44	.21
30	37.00	6.47	.32	.20

Table IV. Concluded

$\psi = 210°$

V, knots	P, hp	P_σ, hp	δ, in.	δ_σ, in.
0	56.24	4.46	0.98	0.10
5	55.68	4.56	.89	.12
10	46.15	4.77	.69	.15
13	43.87	5.03	.32	.13
15	37.94	4.80	.14	.13
20	30.54	5.70	−.37	.19
25	23.73	6.38	−.80	.29
30	16.76	5.80	−1.35	.23

$\psi = 240°$

V, knots	P, hp	P_σ, hp	δ, in.	δ_σ, in.
0	56.24	4.46	0.98	0.10
5	53.13	4.88	.77	.13
10	45.30	6.02	.37	.14
15	25.15	5.89	−.83	.30
20	18.37	4.64	−1.28	.12
25	16.72	4.86	−1.42	.15
30	10.98	4.76	−2.12	.31
35	7.87	4.35	−2.55	.24

$\psi = 270°$

V, knots	P, hp	P_σ, hp	δ, in.	δ_σ, in.
0	56.24	4.46	0.98	0.10
5	57.29	9.56	1.02	.29
10	33.71	6.70	.20	.35
15	17.30	3.66	−1.03	.15
20	13.33	3.62	−1.51	.16
25	11.70	3.77	−1.75	.17
30	7.71	3.77	−2.25	.20
35	5.97	3.65	−2.82	.20

$\psi = 285°$

V, knots	P, hp	P_σ, hp	δ, in.	δ_σ, in.
0	56.24	4.46	0.98	0.10
5	62.74	10.00	1.36	.29
10	17.93	3.79	−.98	.13
18	11.52	4.05	−1.86	.19
23	8.67	6.05	−2.39	.32
29	8.56	4.21	−2.47	.12
34	6.86	4.48	−2.79	.18
38	8.14	5.51	−3.47	.02

$\psi = 300°$

V, knots	P, hp	P_σ, hp	δ, in.	δ_σ, in.
0	56.24	4.46	0.98	0.10
5	61.68	5.42	1.06	.16
8	59.69	13.14	1.29	.41
11	56.25	9.58	1.08	.31
13	50.88	9.33	1.01	.44
18	16.59	5.69	−1.15	.29
20	7.53	5.65	−2.49	.25
25	8.86	6.30	−2.89	.30
30	8.15	6.11	−3.14	.30
35	9.03	5.77	−3.20	.30

$\psi = 315°$

V, knots	P, hp	P_σ, hp	δ, in.	δ_σ, in.
0	56.24	4.46	0.98	0.10
5	58.09	9.69	1.18	.27
10	50.67	11.67	1.00	.41
15	25.34	5.47	−.40	.28
20	16.57	5.48	−1.05	.26
25	5.63	4.92	−2.07	.17
30	4.46	5.54	−2.71	.18
35	8.49	4.87	−3.36	.15

$\psi = 330°$

V, knots	P, hp	P_σ, hp	δ, in.	δ_σ, in.
0	56.24	4.46	0.98	0.10
5	73.85	7.00	1.49	.21
14	46.84	8.52	.59	.35
20	14.36	5.29	−1.51	.08
25	12.31	4.71	−1.68	.07
30	9.96	4.74	−1.97	.07
35	9.37	4.86	−2.16	.11

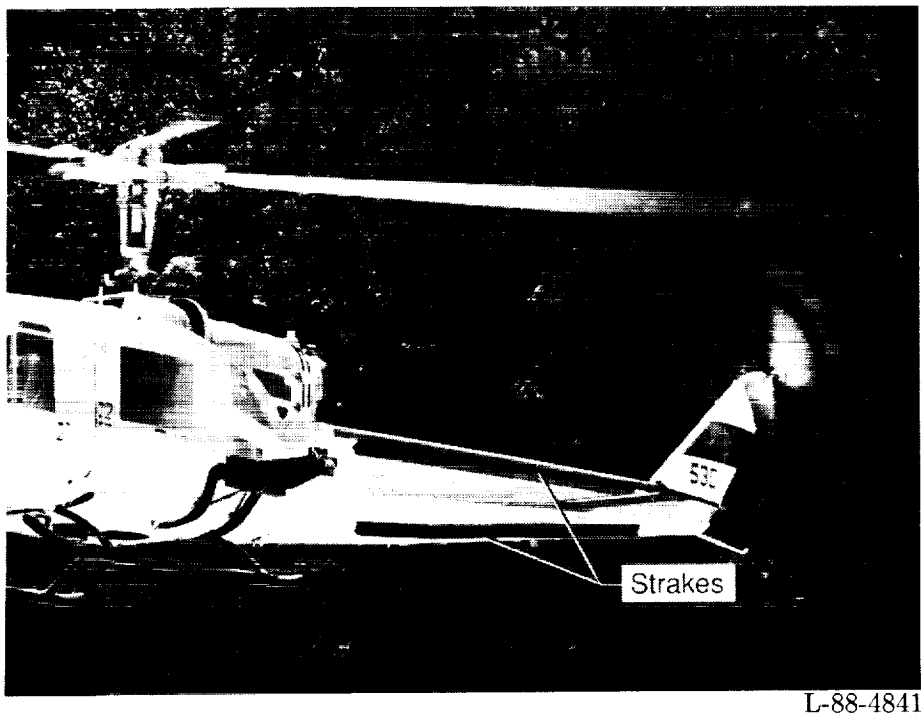

L-88-4841

(a) Test helicopter with upper and lower strakes installed.

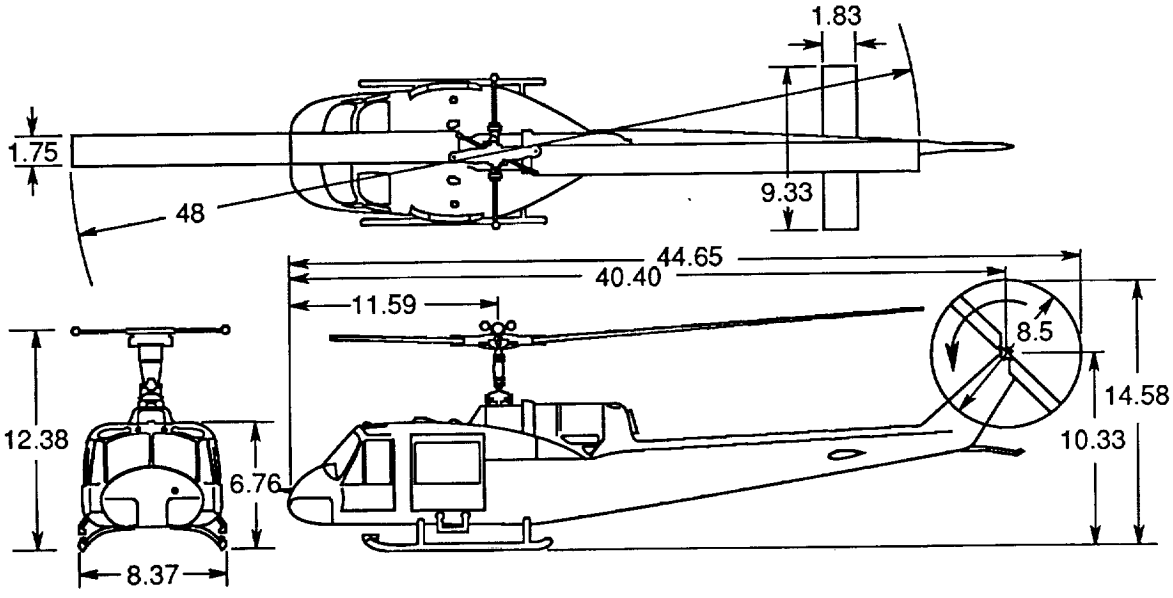

(b) Three-view sketch of test helicopter indicating some of the principal dimensions. Dimensions are in feet.

Figure 1. Test helicopter.

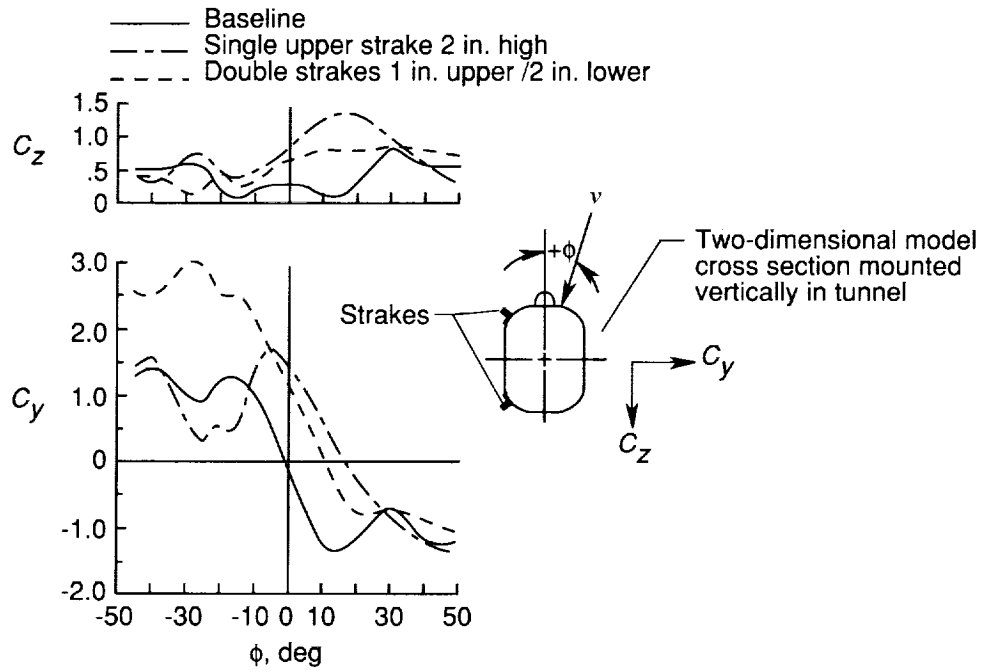

Figure 2. C_z and C_y variation with ϕ on a UH-1 model baseline (no strakes), single-strake, and double-strake model boom configurations (ref. 20).

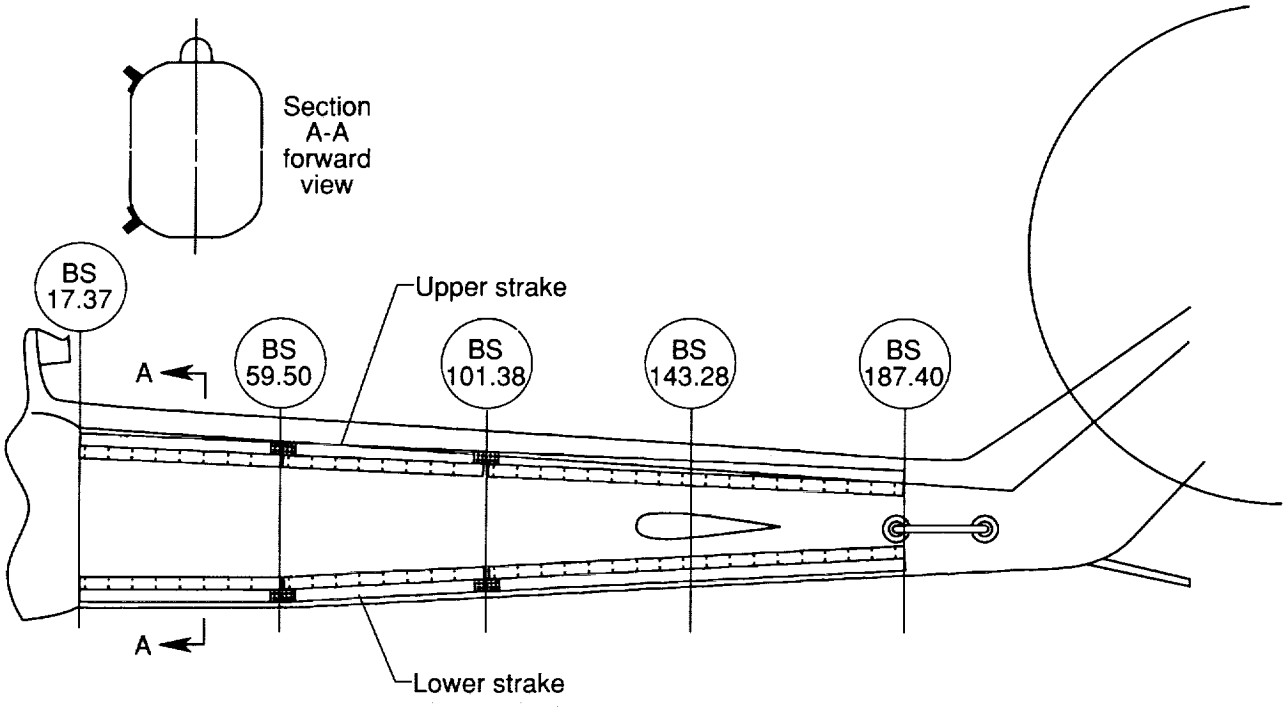

Figure 3. Installation of upper and lower strakes on tail boom of test helicopter.

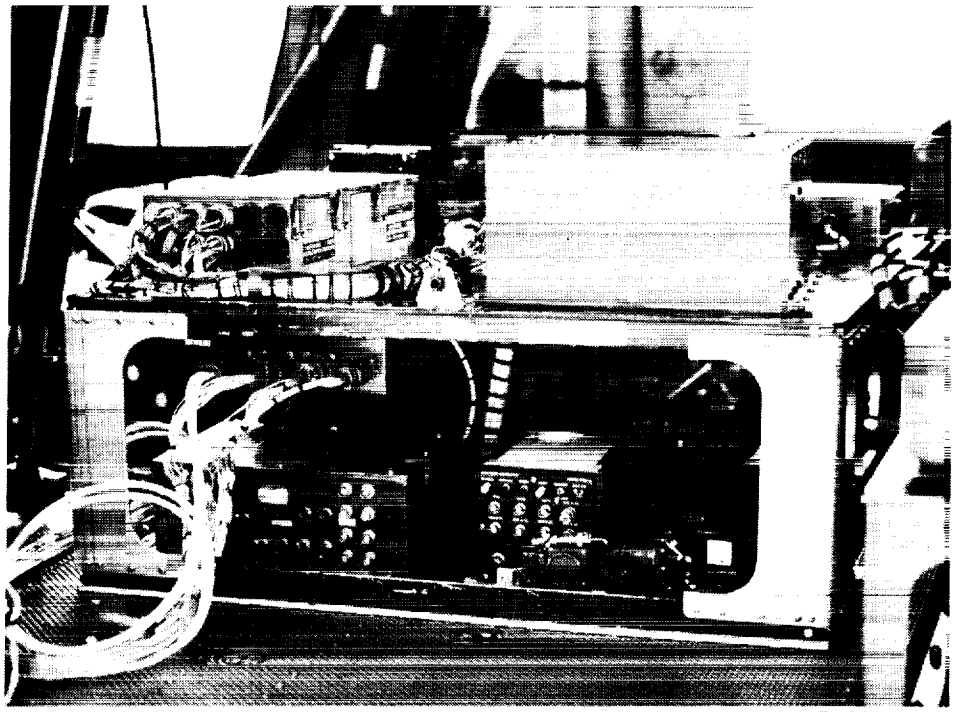

L-88-03656

Figure 4. Instrumentation racks installed behind pilot and copilot seats.

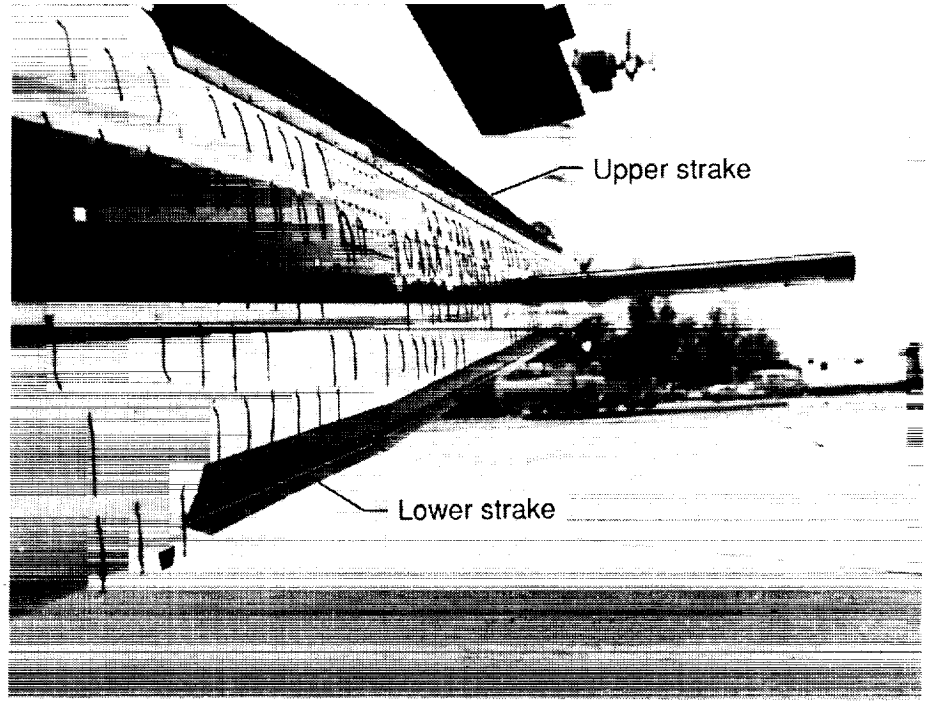

L-89-02452

Figure 5. Tail boom with wool tufts used for flow visualization.

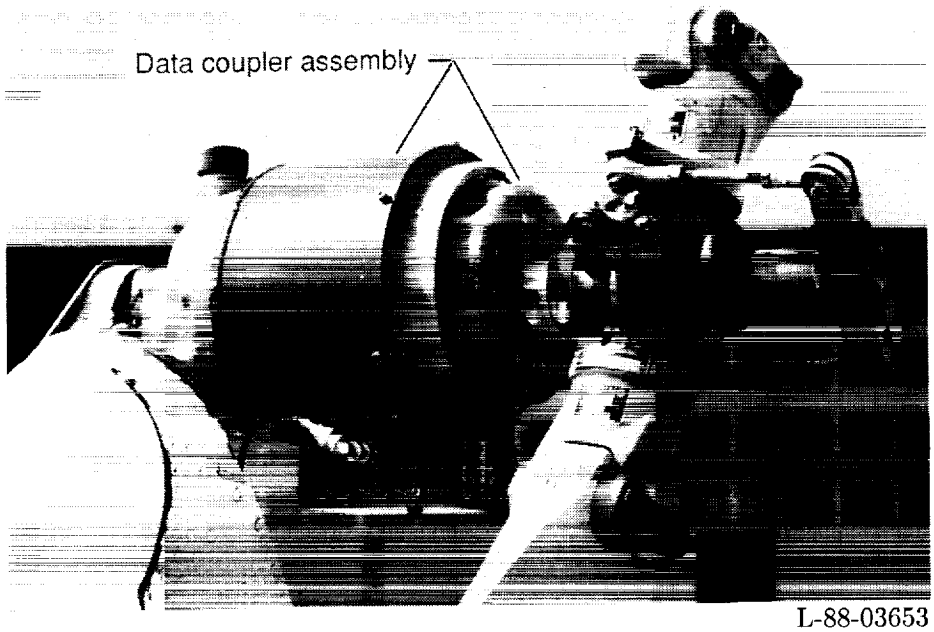

Figure 6. Data coupling device used to telemeter signals from the strain gauges on the tail rotor output drive shaft.

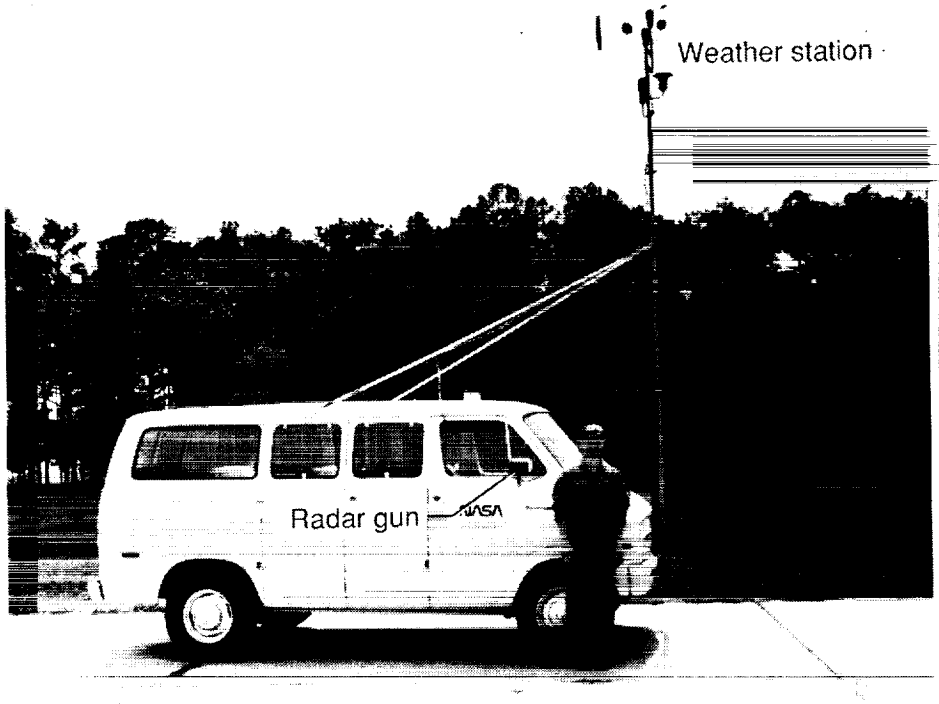

Figure 7. Pace van used to establish airspeed of test helicopter during low-speed sideward flight.

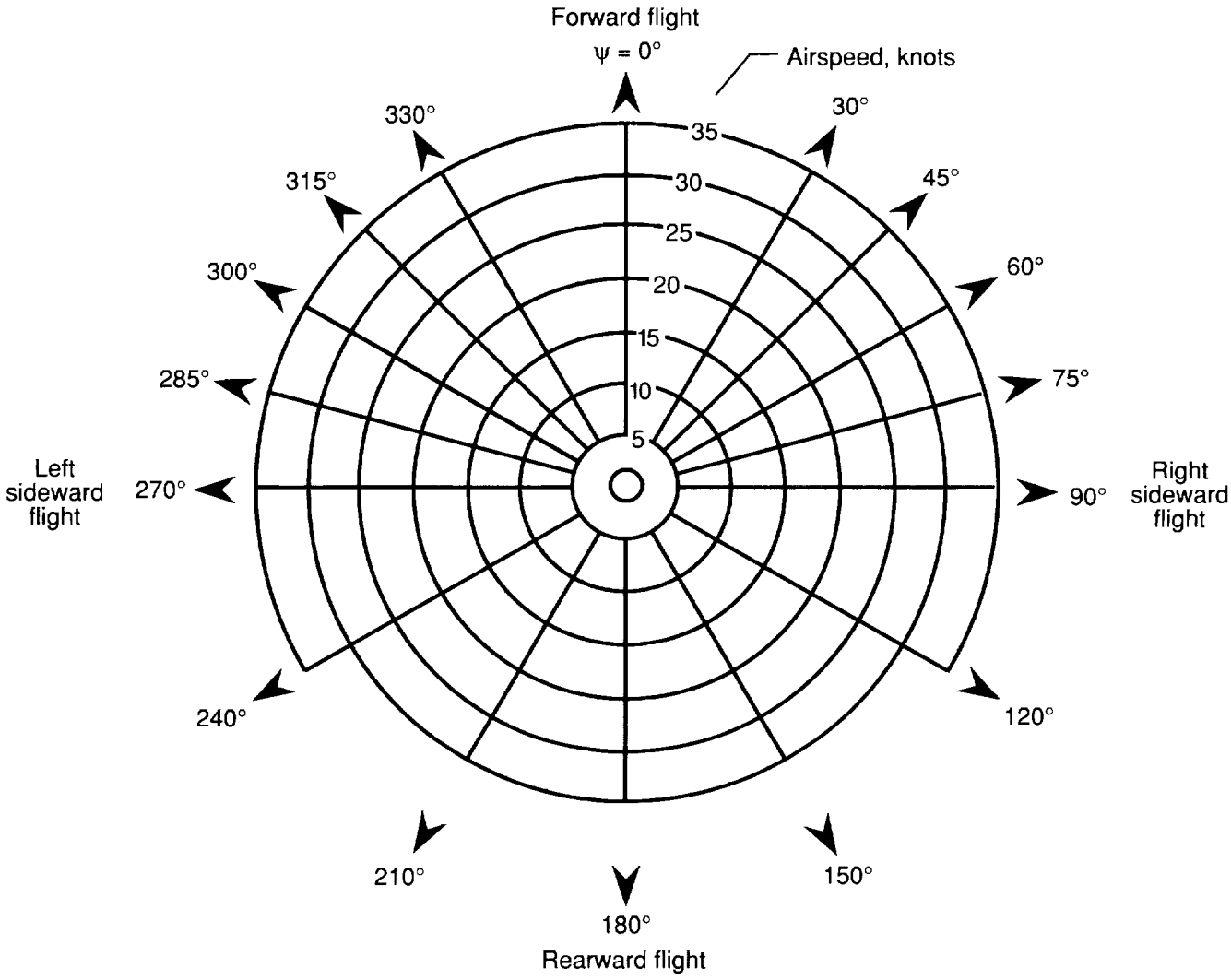

Figure 8. Nominal airspeeds and azimuths investigated during low-speed, crosswind testing.

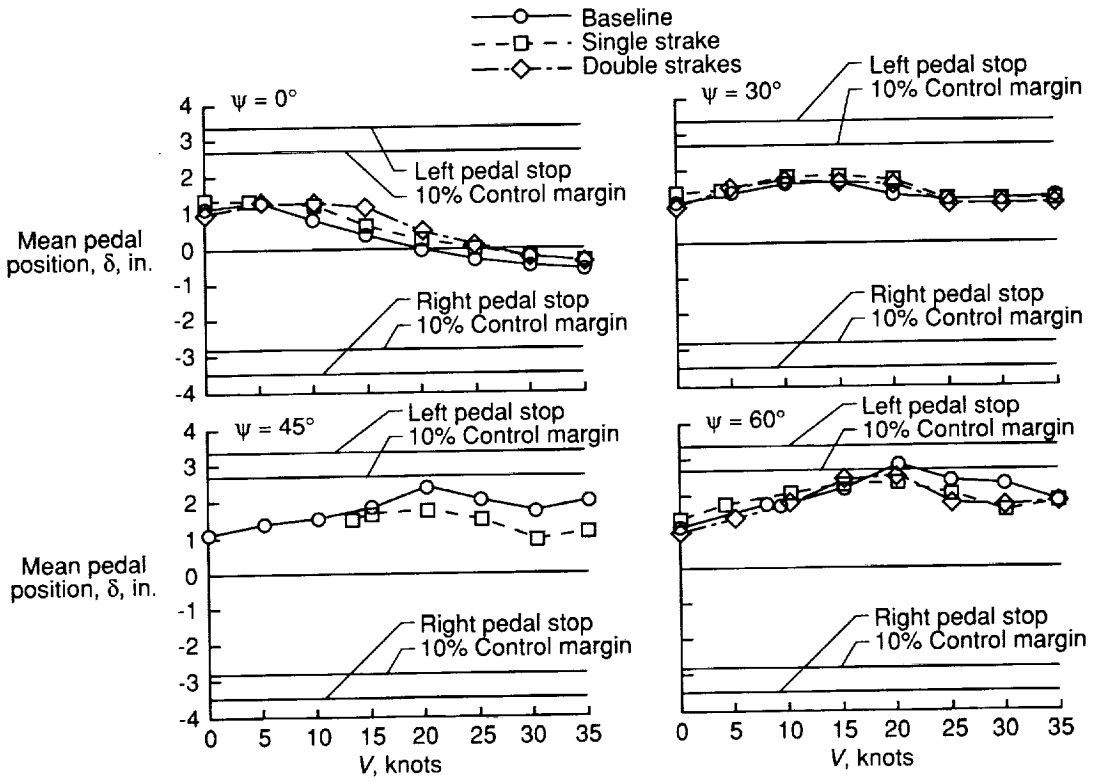

(a) $\psi = 0°$–$60°$.

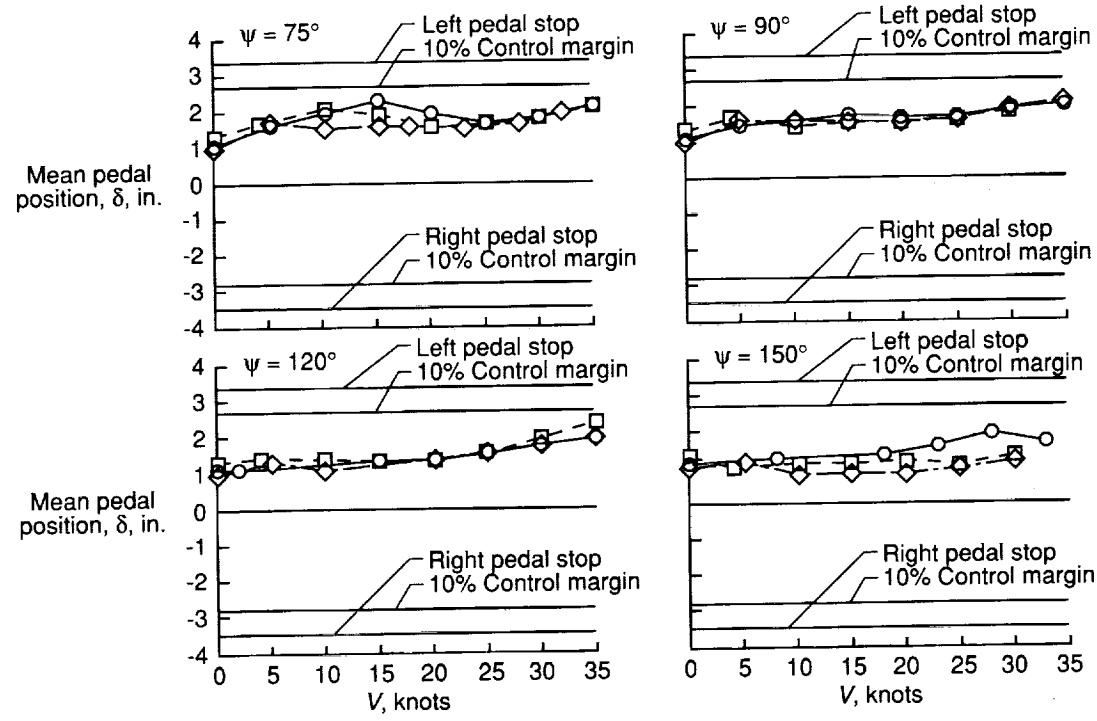

(b) $\psi = 75°$–$150°$.

Figure 9. Mean pedal position as a function of airspeed for $\psi = 0°$–$330°$.

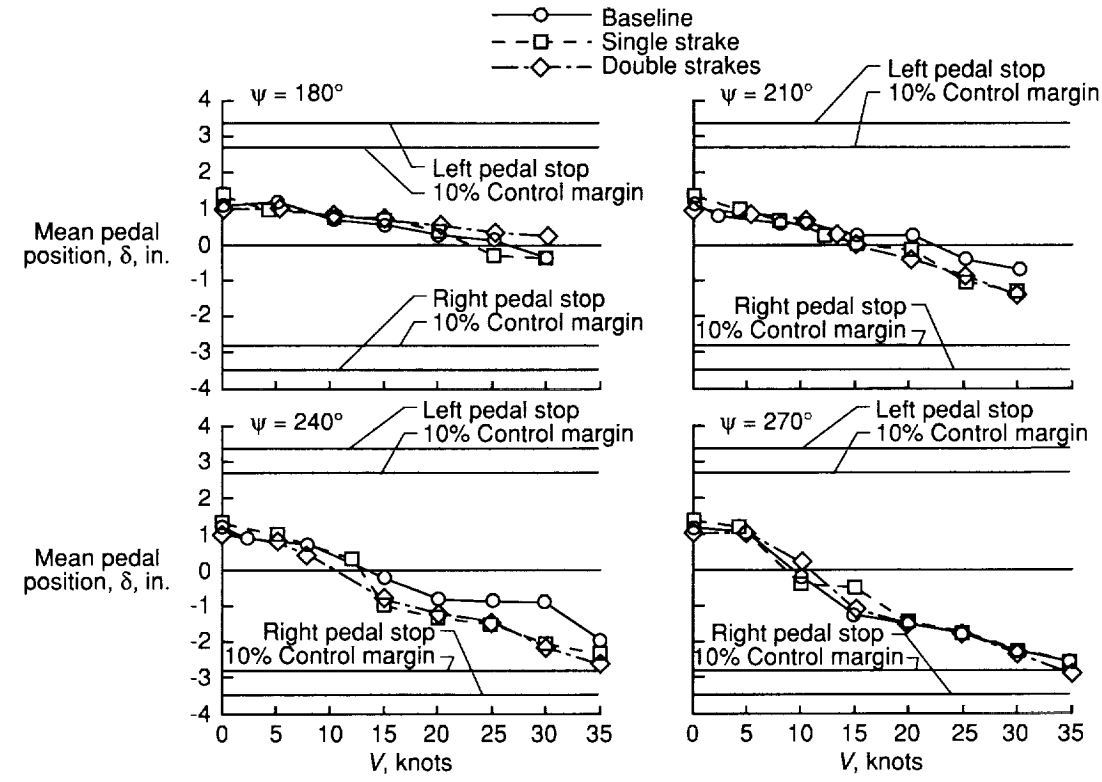

(c) $\psi = 180°$–$270°$.

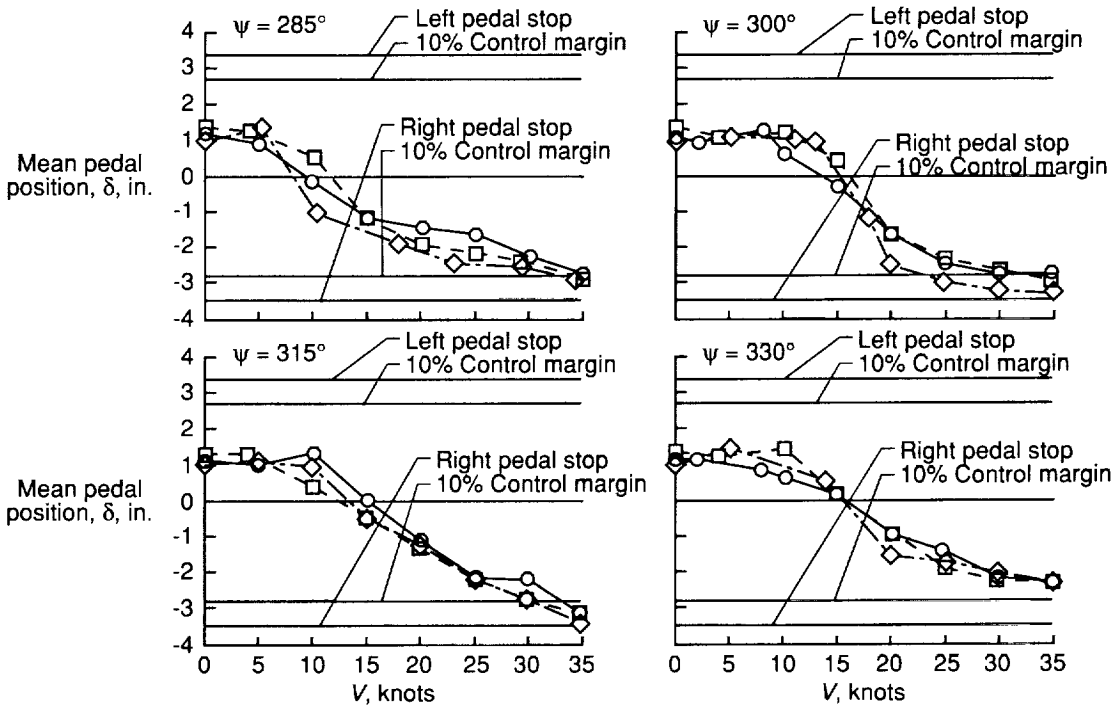

(d) $\psi = 285°$–$330°$.

Figure 9. Concluded.

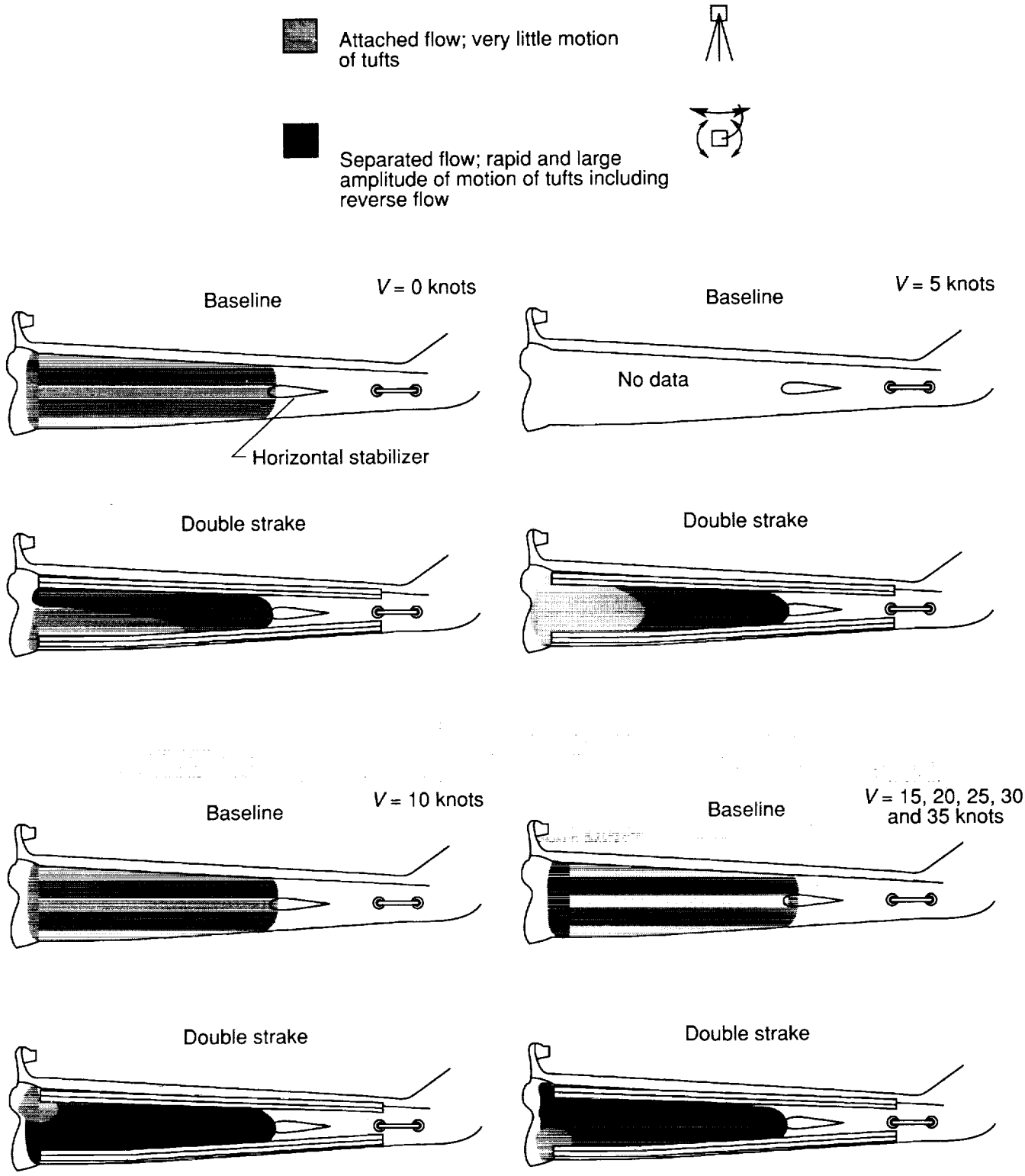

Figure 10. Tail boom airflow patterns for the baseline and double-strake configurations for V = 0–35 knots and $\psi = 60°$. Tufts aft of horizontal stabilizer were not readable.

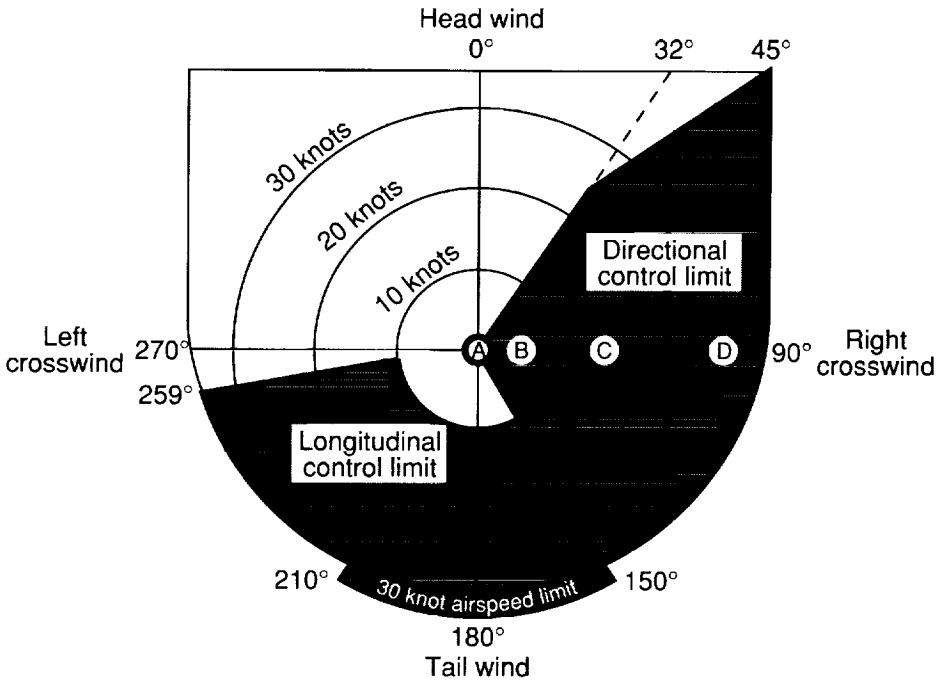

Figure 11. Typical low-speed crosswind control margin in ground effect for the UH-1D, UH-1H, and EH-1H helicopters (ref. 25). Shaded areas indicate control margins may be less than 10 percent of total control travel. Progressing from area D to area A indicates effects of higher gross weight and altitude.

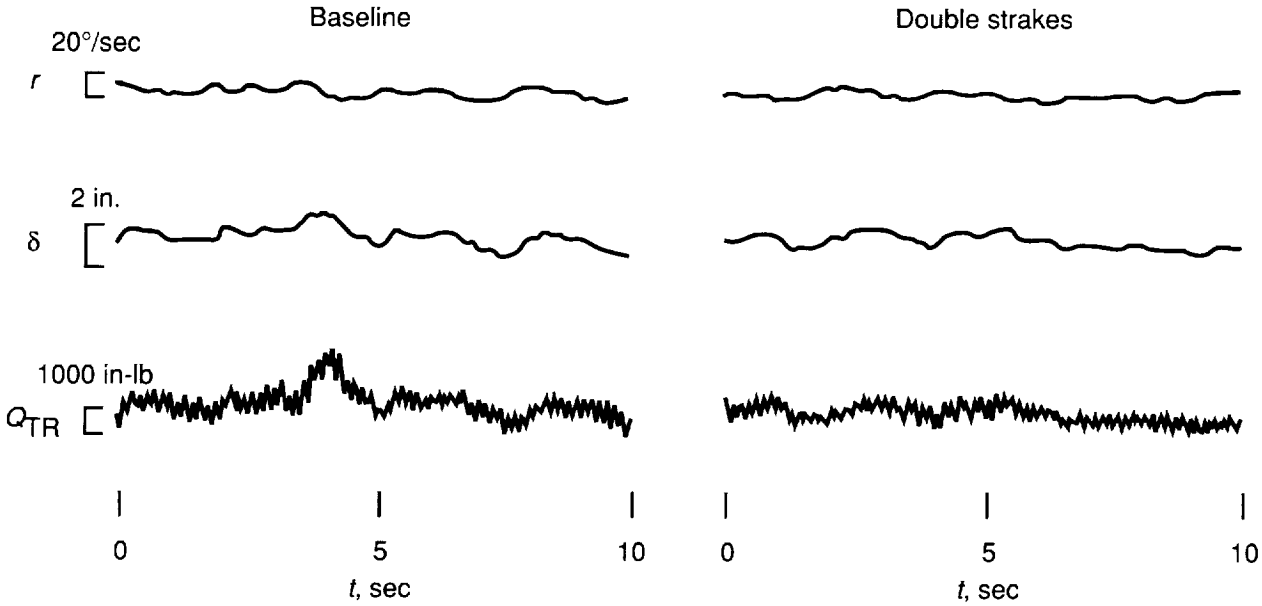

Figure 12. Effect of strakes on precision control while hovering out of ground effect at $\psi = 300°$ and $V = 12$ knots $\pm$ 3 knots.

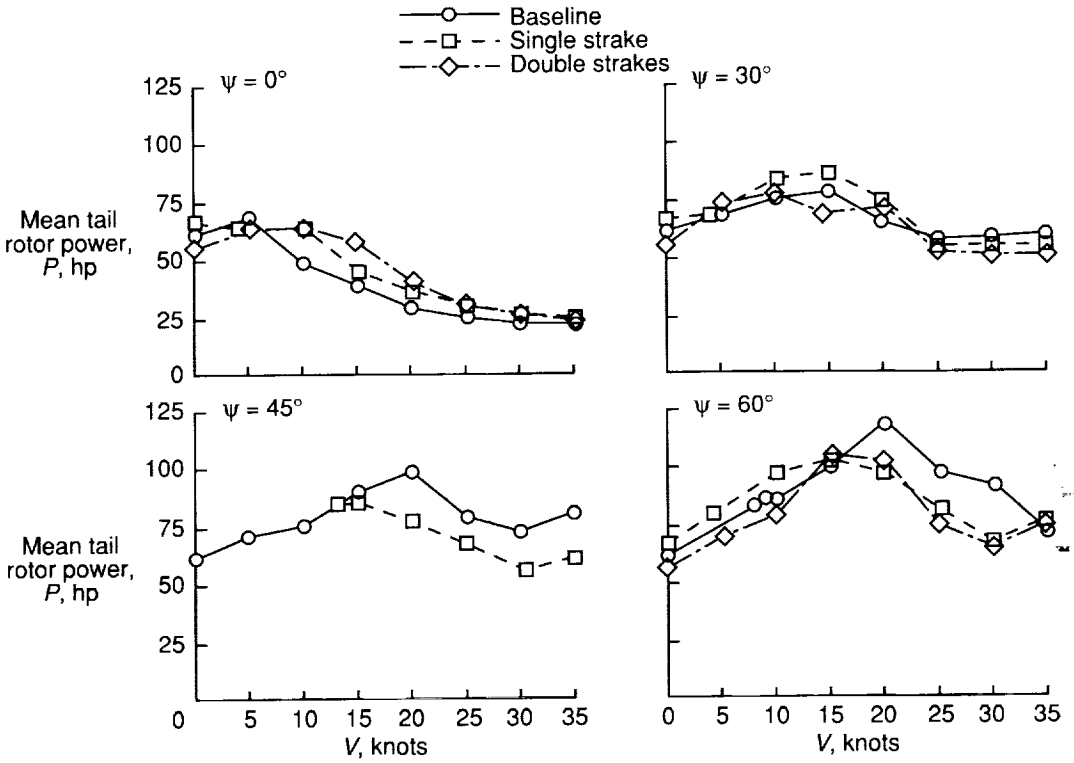

(a) $\psi = 0°$ 60°.

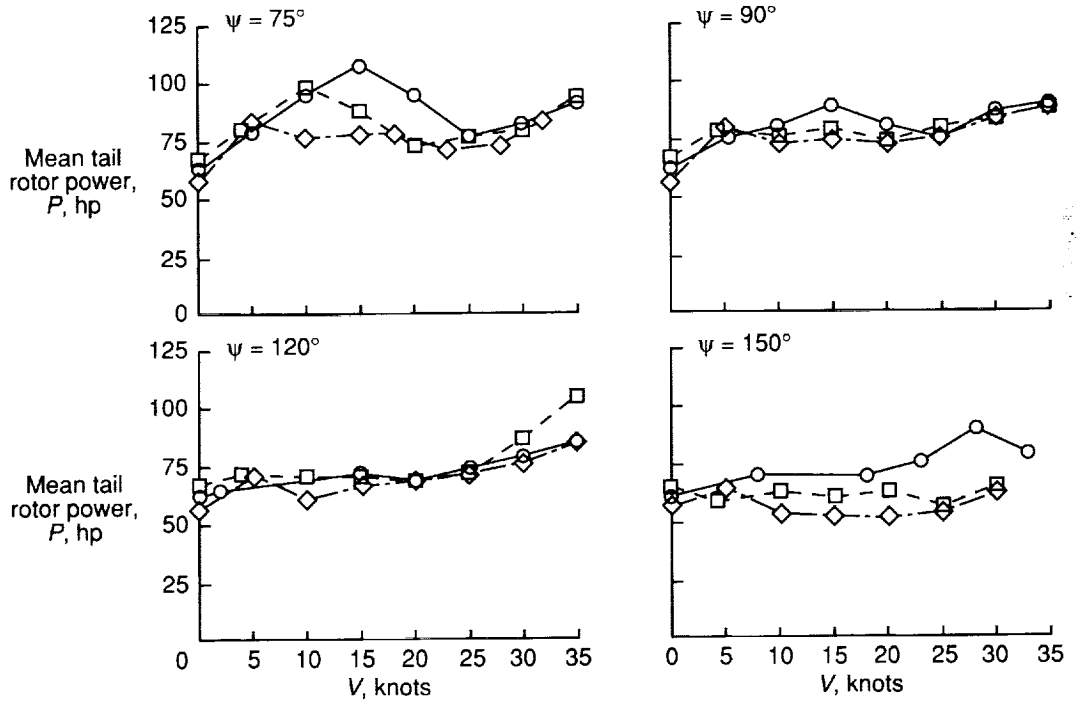

(b) $\psi = 75°$–150°.

Figure 13. Mean tail rotor power as a function of airspeed for $\psi = 0°$–330°.

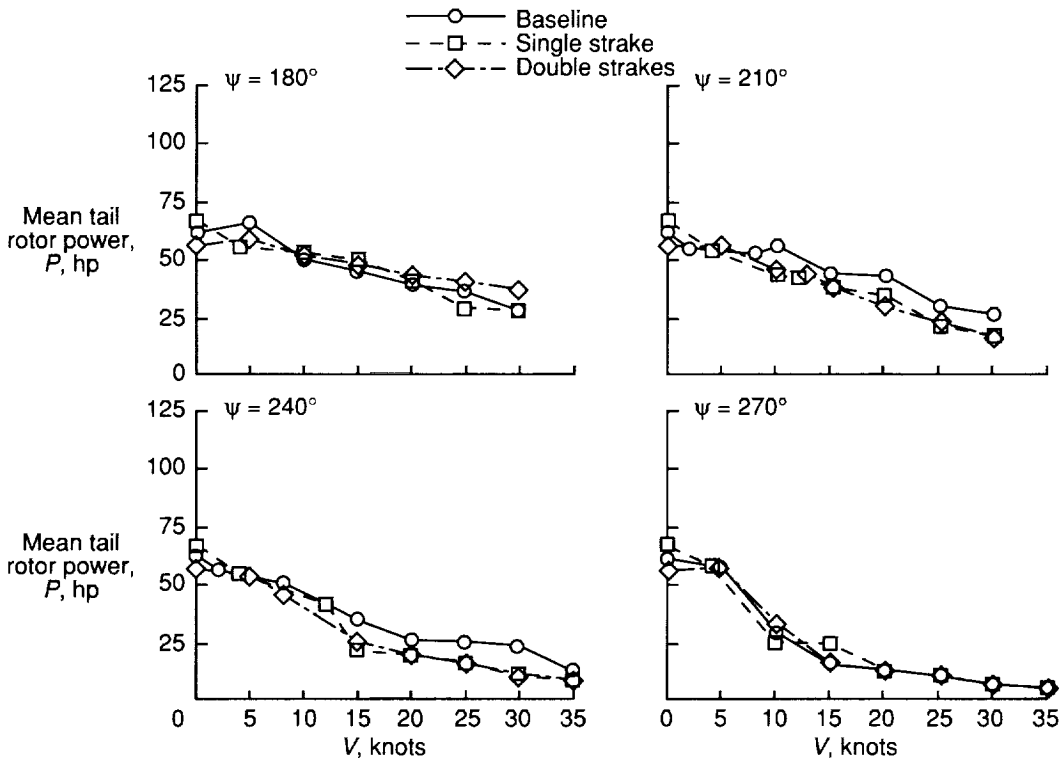

(c) $\psi = 180°$–$270°$.

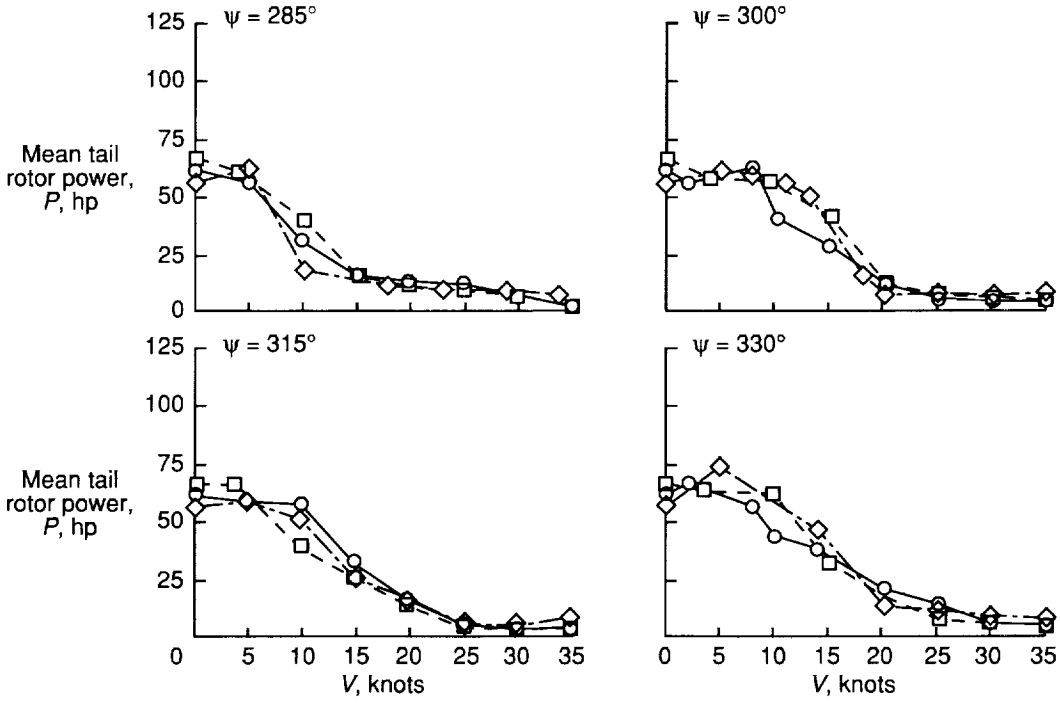

(d) $\psi = 285°$–$330°$.

Figure 13. Concluded.

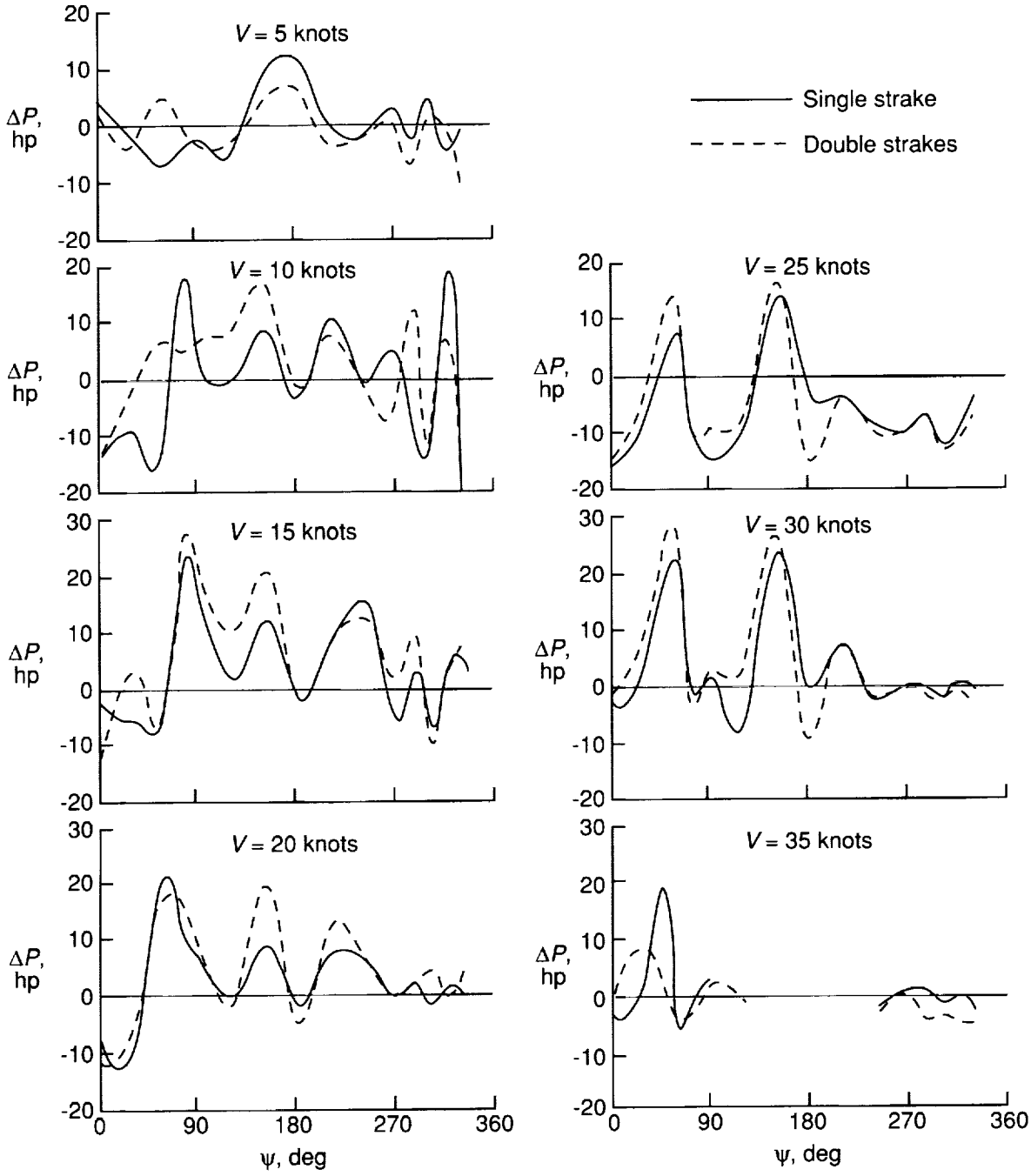

Figure 14. Mean tail rotor power benefit or deficit of single strake and double strakes compared with baseline as a function of wind azimuth and airspeed. Power benefit due to strakes is represented by positive values of ΔP.

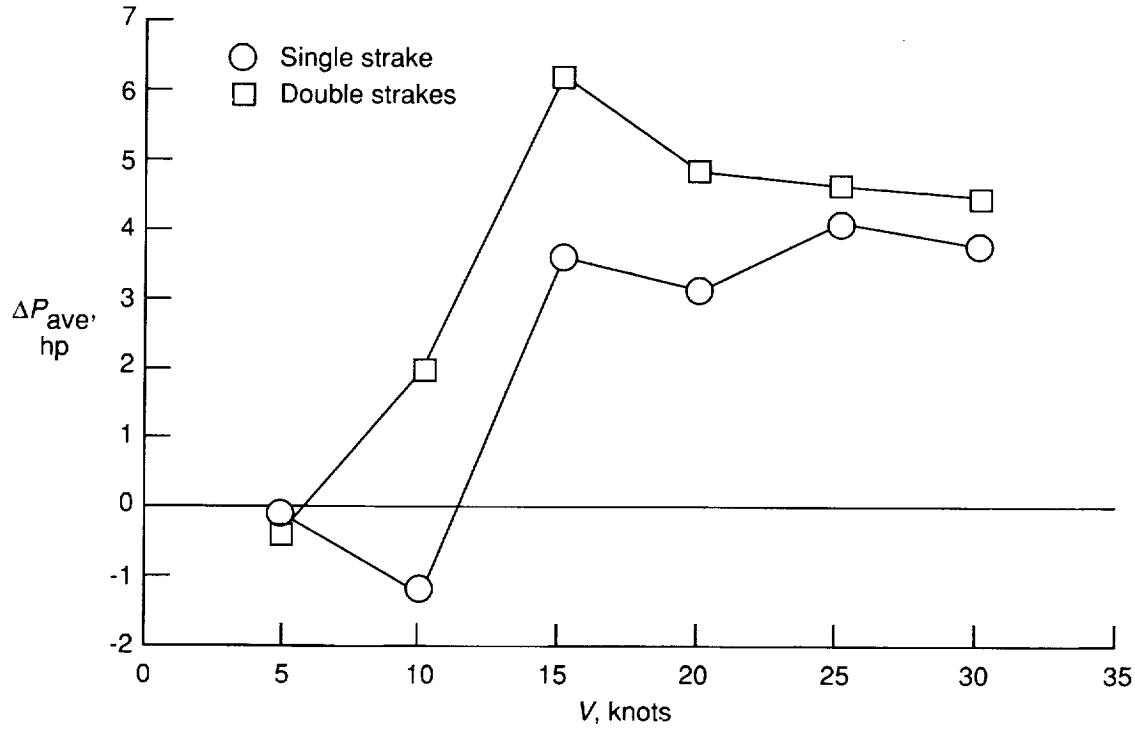

Figure 15. Average benefit or deficit in mean tail rotor power for the strake configurations compared with the baseline. Each data point averaged for the 16 azimuths investigated. Power benefit due to strakes is represented by positive values of ΔP.

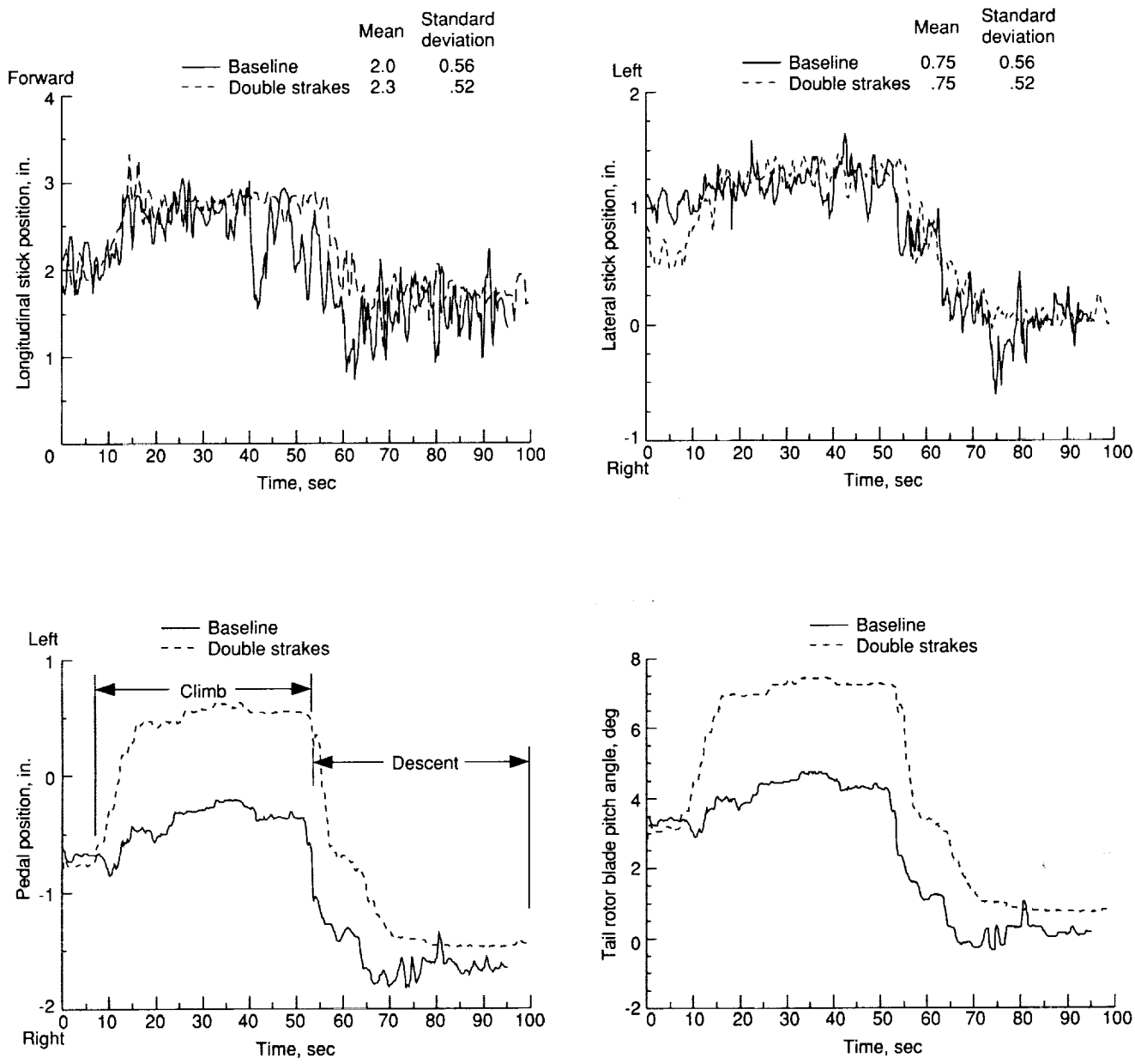

Figure 16. Effect of double strakes during climbing and descending flight (constant airspeed of 60 knots).

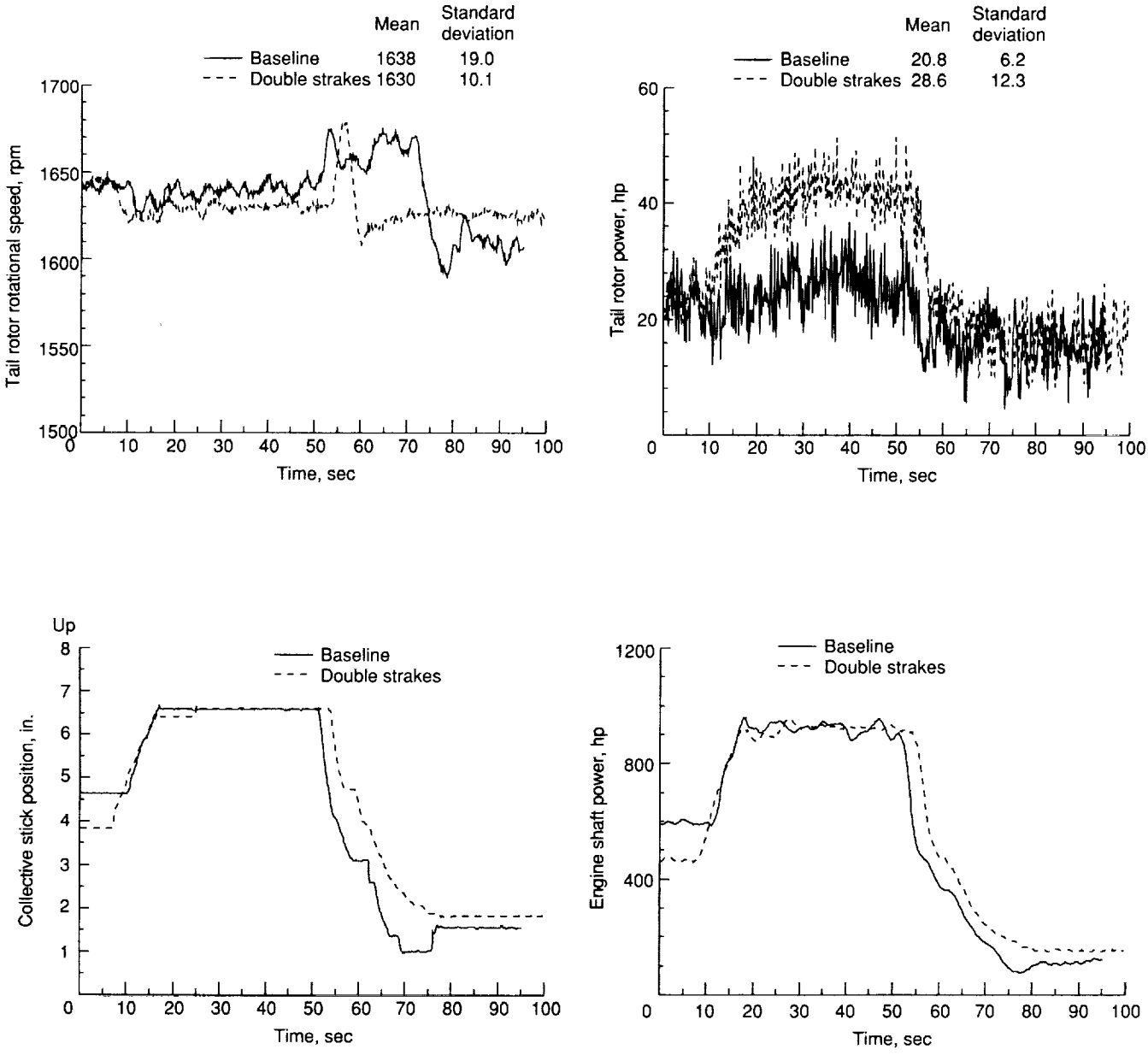

Figure 16. Continued.

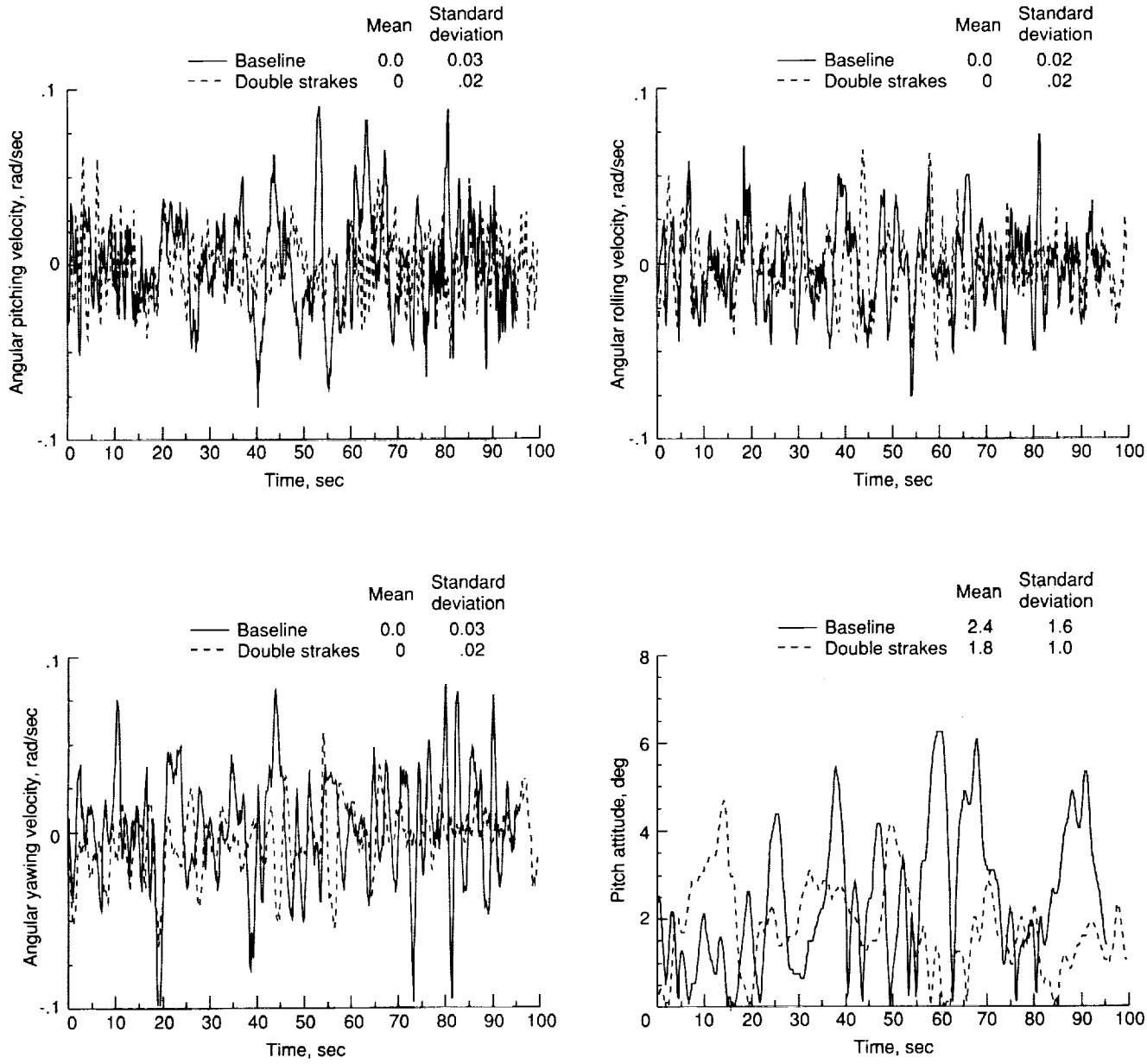

Figure 16. Continued.

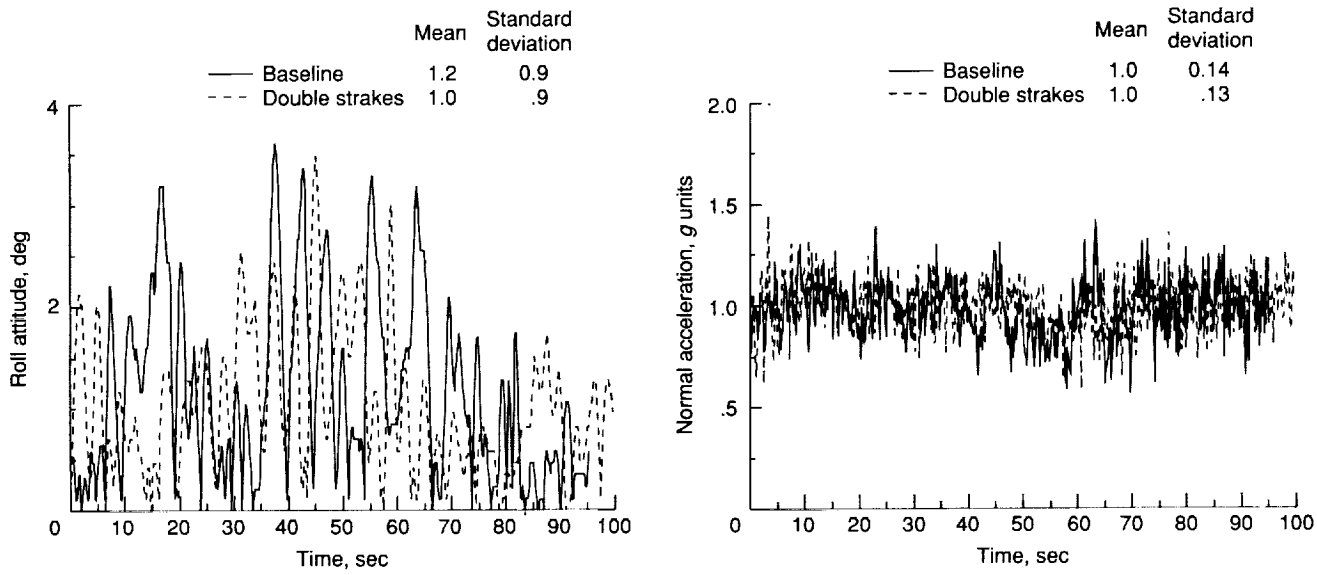

Figure 16. Concluded.

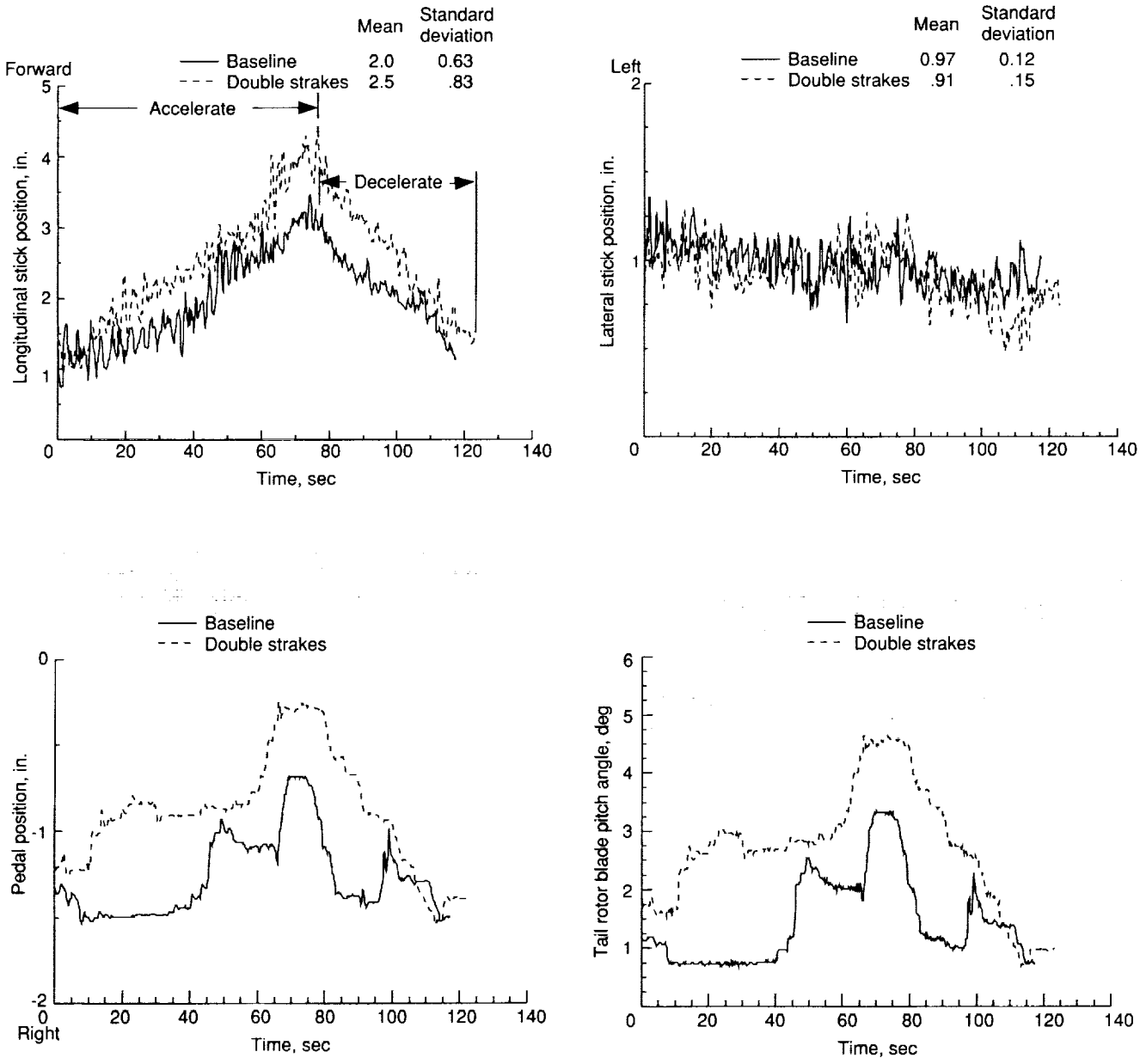

Figure 17. Effect of double strakes during trim-level-flight acceleration and deceleration. Rate of change in airspeed ≤ 1 knot/sec.

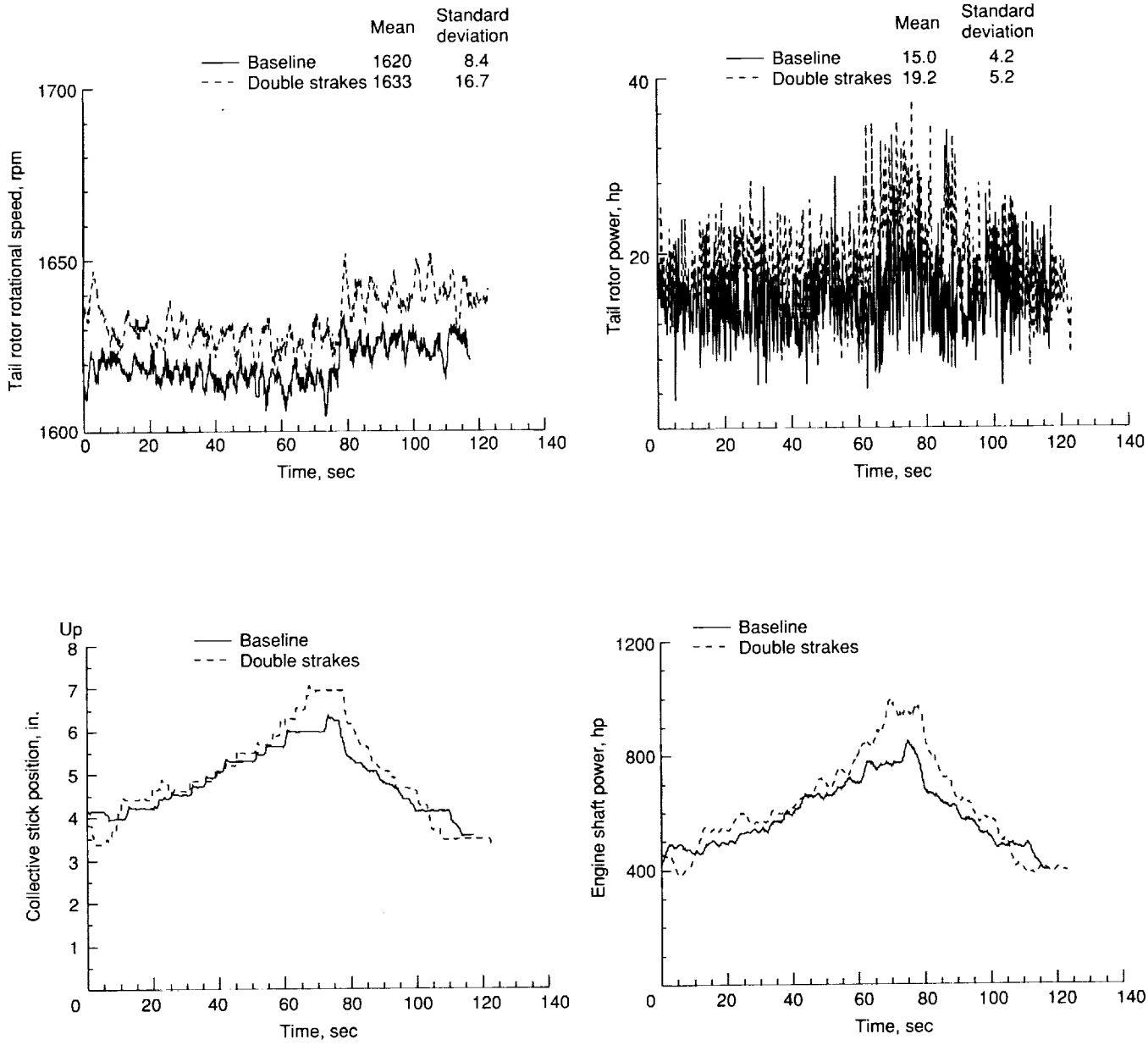

Figure 17. Continued.

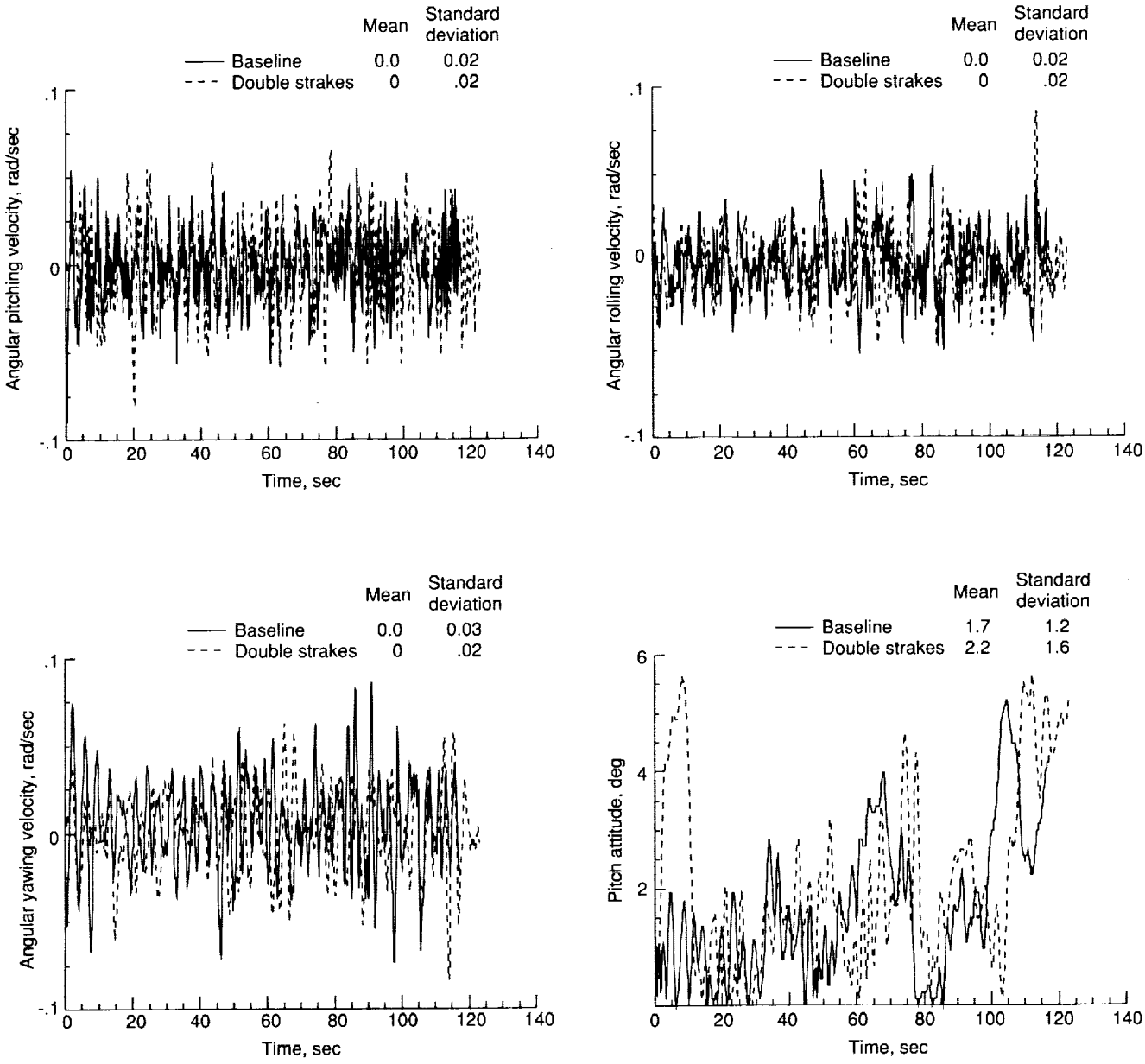

Figure 17. Continued.

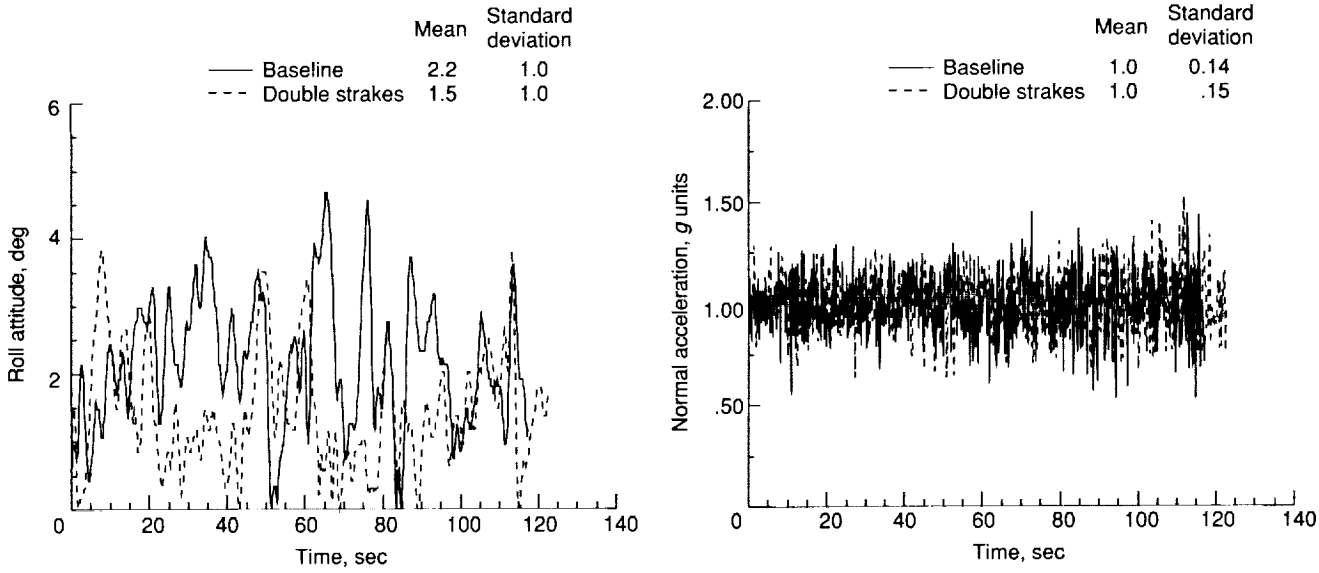

Figure 17. Concluded.

REPORT DOCUMENTATION PAGE

Form Approved
OMB No. 0704-0188

1. AGENCY USE ONLY *(Leave blank)*	2. REPORT DATE	3. REPORT TYPE AND DATES COVERED
	February 1993	Technical Paper

4. TITLE AND SUBTITLE
Flight Investigation of the Effect of Tail Boom Strakes on Helicopter Directional Control

5. FUNDING NUMBERS
1L162211A47A
WU 505-59-36-01

6. AUTHOR(S)
Henry L. Kelley, Cynthia A. Crowell, Kenneth R. Yenni, and Michael B. Lance

7. PERFORMING ORGANIZATION NAME(S) AND ADDRESS(ES)
Joint Research Program Office
Aeroflightdynamics Directorate
U.S. Army Aviation and Troop Command
NASA Langley Research Center
Hampton, VA 23681-0001

8. PERFORMING ORGANIZATION REPORT NUMBER
L-17068

9. SPONSORING/MONITORING AGENCY NAME(S) AND ADDRESS(ES)
National Aeronautics and Space Administration
Washington, DC 20546-0001
and
U.S. Army Aviation and Troop Command
St. Louis, MO 63120-1798

10. SPONSORING/MONITORING AGENCY REPORT NUMBER
NASA TP-3278
ATCOM TR-93-A-003

11. SUPPLEMENTARY NOTES
Kelley: JRPO Langley Research Center, Hampton, VA; Crowell: Now at U.S. Army Europe, Bad Schwalbach, Germany; Yenni: Langley Research Center, Hampton, VA; Lance: Lockheed Engineering & Sciences Co., Hampton, VA.

12a. DISTRIBUTION/AVAILABILITY STATEMENT
Unclassified Unlimited

Subject Category 02

12b. DISTRIBUTION CODE

13. ABSTRACT *(Maximum 200 words)*

A joint U.S. Army/NASA flight investigation was conducted utilizing a single-rotor helicopter to determine the effectiveness of horizontally mounted tail boom strakes on directional controllability and tail rotor power during low-speed, crosswind operating conditions. Three configurations were investigated: (1) baseline (strakes off), (2) single strake (strake at upper shoulder on port side of boom), and (3) double strake (upper strake plus a lower strake on same side of boom). The strakes were employed as a means to separate airflow over the tail boom and change fuselage yawing moments in a direction to improve the yaw control margin and reduce tail rotor power. Crosswind data were obtained in 5-knot increments of airspeed from 0 to 35 knots and in 30° increments of wind azimuth from 0° to 330°. At the most critical wind azimuth and airspeed in terms of tail rotor power, the strakes improved the pedal margin by 6 percent of total travel and reduced tail rotor power required by 17 percent. The increase in yaw control and reduction in tail rotor power offered by the strakes can expand the helicopter operating envelope in terms of gross weight and altitude capability. The strakes did not affect the flying qualities of the vehicle at airspeeds between 35 and 100 knots.

14. SUBJECT TERMS
Helicopter; Fuselage; Tail boom; Blunt bodies; Aerodynamics

15. NUMBER OF PAGES
40

16. PRICE CODE
A03

17. SECURITY CLASSIFICATION OF REPORT	18. SECURITY CLASSIFICATION OF THIS PAGE	19. SECURITY CLASSIFICATION OF ABSTRACT	20. LIMITATION OF ABSTRACT
Unclassified	Unclassified		

NSN 7540-01-280-5500

Standard Form 298(Rev. 2-89)
Prescribed by ANSI Std. Z39-18
298-102

NASA-Langley, 1993